

Anaerobic Corrosion Studies of Carbon Steel Used Fuel Containers

NWMO TR-2010-07

September 2010

Roger C. Newman¹, Steve Wang¹, and Gloria Kwong²

¹University of Toronto

²Nuclear Waste Management Organization (NWMO)

nwmo

NUCLEAR WASTE
MANAGEMENT
ORGANIZATION

SOCIÉTÉ DE GESTION
DES DÉCHETS
NUCLÉAIRES

Nuclear Waste Management Organization
22 St. Clair Avenue East, 6th Floor
Toronto, Ontario
M4T 2S3
Canada

Tel: 416-934-9814
Web: www.nwmo.ca

Anaerobic Corrosion Studies of Carbon Steel Used Fuel Containers

NWMO TR-2010-07

September 2010

Roger C. Newman¹, Steve Wang¹, and Gloria Kwong²

¹University of Toronto

²Nuclear Waste Management Organization (NWMO)

Disclaimer:

This report does not necessarily reflect the views or position of the Nuclear Waste Management Organization, its directors, officers, employees and agents (the "NWMO") and unless otherwise specifically stated, is made available to the public by the NWMO for information only. The contents of this report reflect the views of the author(s) who are solely responsible for the text and its conclusions as well as the accuracy of any data used in its creation. The NWMO does not make any warranty, express or implied, or assume any legal liability or responsibility for the accuracy, completeness, or usefulness of any information disclosed, or represent that the use of any information would not infringe privately owned rights. Any reference to a specific commercial product, process or service by trade name, trademark, manufacturer, or otherwise, does not constitute or imply its endorsement, recommendation, or preference by NWMO.

ABSTRACT

Title: Anaerobic Corrosion Studies of Carbon Steel Used Fuel Containers
Report No.: NWMO TR-2010-07
Author(s): Roger C. Newman¹, Steve Wang¹, and Gloria Kwong²
Company: ¹University of Toronto, ²Nuclear Waste Management Organization (NWMO)
Date: September 2010

Abstract

The Canadian nuclear waste management concept envisages using carbon steel containers as one of the container design options for containing and isolating used nuclear fuel waste in a deep geological repository. Steel corrosion in anticipated repository environments has been studied, but was mostly focused in two main areas: (i) aerobic or oxygen containing environments (both in vapour and liquid phases); and (ii) anaerobic, solution environments. The atmospheric corrosion behaviour of steel in a humid, anaerobic or anoxic environment, is a new topic, with virtually no published data to rely on.

A program of experimental work was undertaken to improve the existing knowledge of anaerobic, atmospheric corrosion of carbon steel. Atmospheric corrosion testing was conducted on carbon steel wires in anoxic atmospheres at 30, 50 and 70°C, over a wide range of relative humidity (30-100% RH), with and without sodium chloride (NaCl) contamination of the wire surfaces. Hydrogen evolved from corrosion was initially monitored with a high sensitivity pressure gauge system and converted to estimated corrosion rate. The sensitivity of such measurements is ca. $0.005 \mu\text{m}\cdot\text{y}^{-1}$. With large amounts of salt contamination, sustained final corrosion rates in the range of 0.01 to $0.8 \mu\text{m}\cdot\text{y}^{-1}$ were observed over test durations of 935 to 1725 hours (tests of such length were not undertaken at 70°C, but higher corrosion rates may be expected). It appears that corrosion occurred at RH values below that associated with saturated NaCl solution. Without salt contamination, the corrosion rates are very low, and can only be detected using a solid-state electrochemical hydrogen sensor. The hydrogen sensor can detect the pressure increase down to a limit of ca. 0.1 Pa, corresponding (depending on the exact procedure) to a corrosion rate as low as ca. $0.0001 \mu\text{m}\cdot\text{y}^{-1}$. The estimated corrosion rates for the degreased and pickled wires were found to be $< 0.01 \mu\text{m}\cdot\text{y}^{-1}$. The use of a quartz crystal microbalance as an alternative way to study such phenomena was found to be unpromising, owing to the lack of long-term stability of the commercial equipment evaluated.

In parallel with the corrosion experiments, corrosion product surface analyses were performed. The oxides formed on the carbon steel surface were examined using (i) scanning electron microscopy coupled with energy dispersive X-ray analysis (SEM/EDX) to determine the structure of the corrosion product films, (ii) X-ray photoelectron spectroscopy (XPS) to identify the chemical composition of the films, and (iii) Raman and Fourier Transform Infrared spectroscopy (FTIR) to study bonding. Oxides formed on steel surfaces were found to consist mostly of Fe_3O_4 , with some Fe III species from traces of air exposure; carbonate was detected on the NaCl contaminated surfaces which had been subject to a degree of prior aerobic corrosion. A high humidity (100%) environment produces more loose surface oxide than a lower humidity environment (75%). The experimental results of this study will be applied to assess the corrosion behaviour of carbon steel containers during the anoxic, unsaturated phase in a deep geological repository.

TABLE OF CONTENTS

	<u>Page</u>
ABSTRACT	v
1. INTRODUCTION	1
2. CORROSION EXPERIMENTS AND HYDROGEN GAS MEASUREMENTS	3
2.1 Overall Design of Corrosion Experiment.....	3
2.2 Material	4
2.3 Preparation of Wire Bundles	4
2.4 Design of the Glass Cell - Pressure Gauge System	5
2.4.1 Experimental Procedure – Pressure Gauge System	7
2.4.2 Leak Test.....	8
2.5 Measurements of Low Rates of Hydrogen Generation Using a Solid-State Electrochemical Hydrogen Sensor in a Copper Corrosion Chamber.....	8
2.5.1 Experimental Procedure – H ₂ sensor	10
2.5.2 H ₂ Sensor Calibration Procedure.....	12
2.5.3 H ₂ Measurement - Pressure Gauge System.....	12
2.6 Analysis of Corrosion Products.....	13
2.6.1 Surface Analysis and Microscopy.....	13
2.6.1.1 X-ray Photoelectron Spectroscopy	13
2.6.1.2 Scanning electron microscopy.....	14
2.6.1.3 Raman spectroscopy	14
2.6.1.4 Fourier Transform Infrared Spectroscopy (FTIR).....	14
2.7 Quartz Crystal Microbalance (QCM)	14
3. RESULTS	15
3.1 Glass Cell – Pressure Gauge Experiments	15
3.1.1 NaCl dipped wires	15
3.1.2 Surfaces with no salt deposit.....	29
3.2 Copper Cell – H₂ Sensor Experiments	34
3.3 Surface Analyses	35
3.3.1 XPS	36
3.3.2 SEM/EDX.....	37
3.3.3 Raman Spectroscopy and Fourier Transform Infrared (FTIR) Spectroscopy	39
4. DISCUSSION OF SURFACE ANALYSIS RESULTS	40
5. FURTHER DISCUSSION AND CONCLUSIONS	57
6. THE WAY FORWARD.....	57

REFERENCES	59
APPENDIX A: Leak test results	61
APPENDIX B: Estimate of corrosion depth corresponding to a pressure change of 0.1 kPa	64
APPENDIX C: Quartz Crystal Microbalance (QCM) Testing	65
APPENDIX D: Preparation of the palladium membrane	67
APPENDIX E: Sample calculation of film thickness estimation of Fe ₃ O ₄ based on pressure measurement.....	68

LIST OF TABLES

	<u>Page</u>
Table 1. Test conditions evaluated in the glass cell - pressure gauge system.	3
Table 2. Nominal composition of iron wire [ppm].....	4
Table 3. Weight gained after NaCl deposition.....	5
Table 4. Saturated salt solutions for humidity control.....	6
Table 5. Test conditions evaluated in the copper cell - H ₂ sensor arrangement.	10
Table 6. Glass cell - pressure gauge experimental results.....	16
Table 7. H ₂ sensor experimental results	34
Table 8. 15 samples examined by surface analyses.....	35
Table 9. Composition data from XPS survey scan spectra.	36
Table 10. Summary of XPS high-resolution spectra data.....	37
Table 11. Composition data from EDX analyses.....	38
Table 12. Summary of Raman and FTIR spectra data.....	39

LIST OF FIGURES

	<u>Page</u>
Figure 1. A conceptual DGR	2
Figure 2a. Wire bundles in the glass cell.....	6
Figure 2b. Glass cell - pressure gauge setup.....	7
Figure 3. Typical leak test results.....	8
Figure 4. Prepared wires in beaker, on top of PTFE.	11
Figure 5. Prepared wires in beaker, placed in the copper cell.	11
Figure 6a. Upper compartment of the copper cell without the palladium membrane.	12
Figure 6b. Upper compartment of the copper cell with the palladium membrane mounted.....	12
Figure 7. Corrosion behaviour of 0.5M NaCl dipped wires tested at 32°C and 68% RH.	17
Figure 8. Corrosion behaviour of 0.5M NaCl dipped wires tested at 32°C and 71% RH.....	17

Figure 9.	Corrosion behaviour of 0.5M NaCl dipped wires tested at 32°C and 75% RH.	18
Figure 10.	Corrosion behaviour of 0.5M NaCl dipped wires tested at 32°C and 100% RH.	18
Figure 11.	Corrosion behaviour of 0.5M NaCl dipped wires tested at 50°C and 30.5% RH.	19
Figure 12.	Corrosion behaviour of 0.5M NaCl dipped wires tested at 50°C and 51% RH.	19
Figure 13.	Corrosion behaviour of 0.5M NaCl dipped wires tested at 50°C and 75% RH.	20
Figure 14.	Corrosion behaviour of 0.5M NaCl dipped wires tested at 50°C and 100% RH.	20
Figure 15.	Corrosion behaviour of 0.5M NaCl dipped wires tested at 70°C and 100% RH.	21
Figure 16.	Corrosion behaviour of 0.05M NaCl dipped wires tested at 50°C and 51% RH.	21
Figure 17.	Corrosion behaviour of 0.05M NaCl dipped wires tested at 50°C and 75% RH.	22
Figure 18.	Corrosion behaviour of 0.05M NaCl dipped wires tested at 32°C and 75% RH.	22
Figure 19.	Corrosion behaviour of 0.5M NaCl dipped wires tested at 32°C and various RH.	23
Figure 20.	Corrosion behaviour of 0.5M NaCl dipped wires exposed to 50°C and various RH.	24
Figure 21.	Corrosion behaviour of 0.5M NaCl dipped wires exposed to 100% RH and various temperatures.	25
Figure 22.	Corrosion behaviour of NaCl dipped wires exposed to 75% RH, 32°C.	26
Figure 23.	Corrosion behaviour of 0.5M NaCl dipped wires exposed to RH \leq equilibrium RH.	27
Figure 24.	Power curve fit of corrosion rates - 0.5M NaCl dipped wires, exposed to 70°C and 100% RH.	28
Figure 25.	Corrosion behaviour of pickled wires exposed to 32°C, 100% RH.	29
Figure 26.	Corrosion behaviour of pickled wires exposed to 50°C, 100% RH.	30
Figure 27.	Corrosion behaviour of pickled wires exposed to 70°C, 100% RH.	30
Figure 28.	Corrosion behaviour of pickled wires exposed to 100% RH.	31
Figure 29.	Linear curve fit of corrosion rates, pickled wires exposed to 32°C and 100% RH.	32
Figure 30.	Exponential curve fit of corrosion rates, pickled wires exposed to 50°C and 100% RH.	32
Figure 31.	Power curve fit of corrosion rates, pickled wires, exposed to 70°C and 100% RH.	33
Figure 32.	SEM images of Sample 2 (3rd and 4th wires) - 0.5M NaCl coated wires.	40
Figure 33.	SEM images of Sample 3 - degreased wires, 50°C, 100% RH.	41
Figure 34.	EDX spectra of Sample 2 - control, 0.5M NaCl coated wires.	43
Figure 35.	EDX spectra of Sample 5 - pickled wires (II), 50°C and 100% RH.	44
Figure 36.	XPS high resolution spectra of Sample 5 - pickled wires (II), 50°C, 100% RH.	47
Figure 37.	XPS analysis of raw steel wires.	49
Figure 38a.	Raman spectrum of Sample 4 – pickled wires, 50°C, 100% RH.	50
Figure 38b.	Raman spectrum of Sample 4 – pickled wires, 50°C, 100% RH.	50
Figure 38c.	Raman spectrum of Sample 4 – pickled wires, 50°C, 100% RH.	51
Figure 39a.	SEM images of Sample 7 – 0.5M NaCl dipped wires, 50°C, 75% RH.	52
Figure 39b.	EDX spectra of Sample 7 – 0.5M NaCl dipped wires, 50°C, 75% RH.	53
Figure 40a.	Raman spectrum of Sample 6 - 0.5M NaCl coated wires, 50°C, 75% RH (no rinse).	54
Figure 40b.	Raman spectrum of Sample 6 – 0.5M NaCl coated wires, 50°C, 75% RH.	54
Figure 41.	FTIR spectrum of Sample 10 – 0.5M NaCl coated wires, 100% RH, 50°C(rinsed)..	55
Figure 42a.	Raman spectrum of Sample 11 - pickled wires, 70°C, 100% RH.	56
Figure 42b.	Raman spectrum (average)of Sample 11 – pickled wires, 70°C, 100%RH.	56

1. INTRODUCTION

The Canadian nuclear waste management concept envisages using a carbon steel container as a primary engineered barrier for containing and isolating used nuclear fuel in a deep geological repository (DGR) (McMurry et al. 2003) as illustrated in Figure 1. A deep geological repository is an approach being considered for long-term management of nuclear fuel waste in many countries such as Sweden, Switzerland, the United Kingdom, Canada and the United States. In a DGR, used nuclear fuel would be sealed in durable metal containers and placed in an engineered repository constructed deep in stable host rock. The layout of the Canadian repository would be a network of tunnels and placement rooms designed to accommodate the rock structure and stresses, the groundwater flow system, and other subsurface conditions at the site. A clay buffer material would surround each container, and backfill material and other seals would close off the rooms. The rock and groundwater that surround the repository would provide stable mechanical and chemical conditions that would also promote containment of the wastes for long times.

Steel corrosion in anticipated repository environments has been studied, but was mostly focused in two main areas: (i) aerobic or oxygen containing environments (both in vapour and liquid phases); and (ii) anaerobic, solution environments (King 2007). The long term behaviour of steels, in particular the less corrosion-resistant carbon steel, in humid, non-immersed, anaerobic or anoxic conditions, has not been studied. The lack of such data may be due to the relatively slow corrosion rates and difficulties in precise measurements. This condition (i.e. humid and anoxic) has nonetheless been repeatedly reported in various Canadian sedimentary host rock studies to span from thousands to millions of years after DGR closure (Mazurek, 2004, King, 2007). The need for addressing the anaerobic steel corrosion issue in humid, vapour phase conditions is evident.

This objective of this work program was to improve the existing understanding of anaerobic, unsaturated corrosion of carbon steel with the following underlying considerations:

1. study the kinetics and mechanism of long term anaerobic, unsaturated corrosion of carbon steel as a function of relevant variables;
2. evaluate the effect of time-dependent oxide film formation on the corrosion rate.

At the time the proposal was prepared, it was anticipated that anoxic atmospheric corrosion might show a kind of feedback or autocatalysis effect, where the development of a porous, conducting corrosion product enhances the kinetics of hydrogen evolution and thus the corrosion rate. In the event, no evidence for such effects was observed, so this aspect was not pursued in detail.

The program started in November 2007, with the initial aims being to evaluate the optimal corrosion cell setup, hydrogen detection techniques and testing protocols. Two approaches were taken to monitor the hydrogen evolved from anaerobic corrosion of steel. In the first, a corrosion system equipped with a high sensitivity pressure gauge was constructed to measure, directly, the amount of hydrogen evolved. In cases where pressure increases were not detectable by the pressure gauge, a solid-state electrochemical hydrogen sensor was employed to measure traces of hydrogen evolved. This second detection method had a sensitivity of at least an order of magnitude better than the pressure gauge system. Intensive data collection using the preferred techniques continued until February 2010. In parallel with the corrosion experiments, the structures and chemical compositions of the oxides formed during the anaerobic corrosion studies were analyzed using various surface analyses. This report presents the experimental details of the hydrogen measurements and discusses the results in the context of the probable carbon steel performance in the expected Canadian repository conditions.

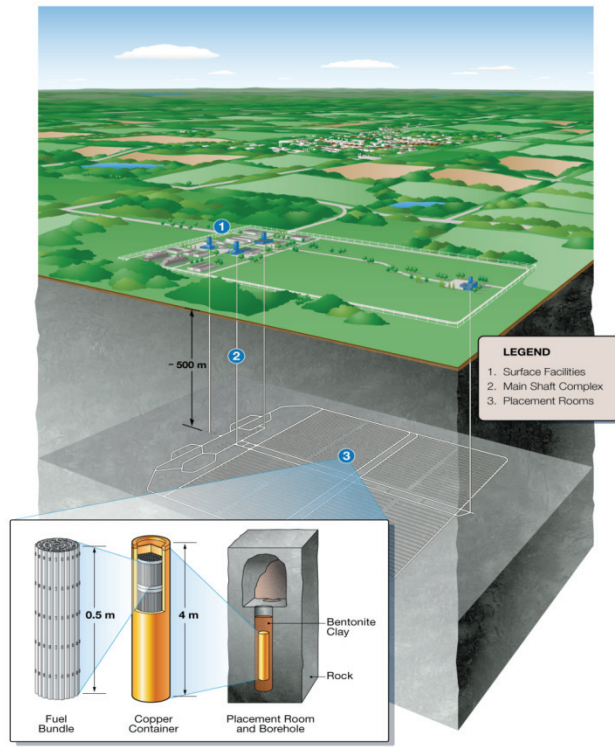


Figure 1: A conceptual DGR

2. CORROSION EXPERIMENTS AND HYDROGEN GAS MEASUREMENTS

2.1 Overall Design of Corrosion Experiment

Hydrogen generation from a large surface area of carbon steel wires has been the primary means to monitor the corrosion behaviour of carbon steel under anaerobic unsaturated conditions. An initial glass-cell setup, measuring hydrogen using fluid displacement, was unsuccessful, owing to the imprecise response of the mercury manometer to very small pressure changes. Pressure monitoring was then pursued in a similar glass system, but using a high-sensitivity digital pressure gauge. After a series of evaluations, this setup was concluded to have satisfactory sensitivity and leak tightness, and has provided a controlled atmosphere for use in this atmospheric corrosion study. The effects of fundamental variables such as relative humidity (RH), surface condition including salt deposition, and temperature have been studied. Table 1 summarizes the test conditions studied in the series of corrosion experiments.

Table 1: Test conditions evaluated in the glass cell - pressure gauge system

Test Condition	Duration (h)
Wires precorroded with 0.5M NaCl then dried	
Test #1 68% RH, 32°C	1347
Test #2 71% RH, 32°C	935
Test #3 75% RH, 32°C	1730
Test #4 100% RH, 32°C	1270
Test #5 30.5% RH, 50°C	1962
Test #6 51% RH, 50°C	1053
Test #7 75% RH, 50°C	450
Test #8 100% RH, 50°C (I)	237
Test #9 100% RH, 50°C (II)	1725
Test #10 100% RH, 70°C	213
Wires pre-corroded with 0.05M NaCl then dried	
Test #11 51% RH, 50°C	1867
Test #12 75% RH, 50°C	2326
Test #13 75% RH, 32°C	3355
As-cleaned surfaces	
Test #14 100% RH, 32°C	379
Test #15 100% RH, 50°C (deaerated with N ₂ / H ₂)	591
Test #16 100% RH, 50°C (deaerated with N ₂)	615
Test #17 100% RH, 50°C (reused wires from pickled test at 74.1% RH, 70°C)	309
Pickled surfaces	
Test #18 75% RH, 32°C	1171
Test #19 75% RH, 50°C	331
Test #20 74.1% RH, 70°C	1121
Test #21 100% RH, 32°C	1337
Test #22 100% RH, 50°C	1002
Test #23 100% RH, 50°C (reused wires from 75% RH, 50°C test)	688
Test #24 100% RH, 70°C	1006

2.2 Material

“Iron” wire of 0.25 mm diameter and 99.5% purity, supplied by Goodfellow Cambridge, was used in this study. Its nominal composition is listed in Table 2.

Table 2: Nominal composition of iron wire [ppm]

Fe	Al	Ca	Co	Cr	Cu	Mn	Ni	Sn	C	P	S
balance	30	30	100	100	100	4000	200	50	<800	<600	<600

For comparison, SA516 Gr. 70 has the following nominal composition: C: max 0.28%, Mn: 0.85 to 1.2%, P: max 0.035%, S: max. 0.035%, Si: 0.15 to 0.4%.

Although the supplier refers to the wire as ‘iron’, it is a low-carbon steel, and as such should represent the corrosion performance of any fairly similar steel. We note that Smart has shown similar corrosion rates for different materials and product forms in immersion testing (Smart et al. 2006)

2.3 Preparation of Wire Bundles

A total length of 130 m of steel wire, corresponding to 0.102 m² surface area (the same exposed surface area as the UK anaerobic corrosion experiment - Peat et al. 2001) was used for each exposure. The wire was cut into 50 mm lengths and 100 pieces of the cut wires were tied with two PTFE rings to form a bundle. A total of 26 bundles were placed into the glass cell.

Tied bundles were then degreased in acetone ultrasonically for 30 minutes, followed by a thorough rinse with water. The bundles were then further ultrasonically rinsed in deionized water three more times, each time for 3 minutes.

Following rinsing, one of three surface finishes was applied, namely (i) salt deposit or pre-corroded with NaCl; (ii) as-cleaned; and (iii) pickled; the corresponding preparation procedures are described below:

- (i) Pre-corroded with NaCl (Tests #1 to #13): after the rinsing with de-ionized water, the wires were ultrasonically soaked in 250 mL of 0.5M (Tests # 1 to #10) or 0.05M NaCl solution (Tests #11-13) for 10 minutes at room temperature. NaCl soaked wires were then dried in a vertical position in an oven at 50°C for 12 hours or more. The amounts of NaCl deposited on the wires in each test are tabulated in Table 3. This procedure should be considered as a combination of NaCl deposition and pre-corrosion. The results indicate that the deleterious effect of salt deposited on the wires is much higher with the use of the 0.5M NaCl solution than the 0.05M NaCl solution.
- (ii) As-cleaned (Tests #14 to #17): after the rinsing with de-ionized water, the wire bundles were placed in anhydrous ethanol and then dried with ambient-temperature flowing air.
- (iii) Pickled (Tests # 18 to #24): after the rinsing in de-ionized water, the wire bundles were soaked in 10% HCl solution for 5 minutes, then ultrasonically rinsed using de-ionized water

three more times, each time for 3 minutes. After that, the bundles were rinsed in anhydrous ethanol and then dried with flowing air.

Table 3: Weight gained after NaCl deposition

Test #	Test Conditions	Weight gained
Pre-corroded with 0.5M NaCl		
1	68% RH, 32°C	0.81 g
2	71% RH, 32°C	0.66 g
3	75% RH, 32°C	0.62 g
4	100% RH, 32°C	0.74 g (average)
5	30.5% RH, 50°C	0.74 g
6	51% RH, 50°C	0.90 g
7	75% RH, 50°C	0.80 g
8	100% RH, 50°C	0.74 g (average)
9	100% RH, 50°C(II)	0.67 g
10	100% RH, 70°C	1.14 g
Pre-corroded with 0.05M NaCl		
11	51% RH, 50°C	0.75 g
12	75% RH, 50°C	0.68 g
13	75% RH, 32°C	0.18 g

2.4 Design of the Glass Cell - Pressure Gauge System

Photographs of the assembled corrosion cell/pressure gauge system are shown in Figures 2a and 2b. The cell has an inner volume of 170 mL and is equipped with 3 openings, Openings 1 and 2, with an inside diameter of 1 mm, are provided for cell deaeration and pressure relief. Opening 3 connects the digital pressure gauge to the corrosion cell using 2 mm diameter stainless steel tubing about 500 mm long. The connection of the pressure gauge to Opening 3 was sealed with a rubber ring, PTFE tape, and Dow Corning high vacuum grease. Two models of digital pressure gauges were used in the experiments : (i) GE Druck DPI 104 – a micro-processor controlled digital pressure gauge with 0.01 kPa resolution and 0.05% full scale accuracy; and (ii) Accu-Cal Plus digital precision test gauge - supplied by 3D Instruments, with 0.04% full scale accuracy. Both pressure gauges have operation pressure range at 30 psia.

The wire bundles rested on a PTFE screen above the solution used for humidity control. Different solutions were used for humidity control. They are listed, along with their literature values of equilibrium relative humidity, in Table 4. Temperatures were controlled through the use of a water bath. A HH41 thermistor thermometer equipped with ON-403-PP immersion thermistor probe (manufactured by Omega Engineering Inc.) was used to provide continuous monitoring of temperature of the water bath. The thermistor has a resolution of 0.01°C, with an overall accuracy of $\pm 0.2^\circ\text{C}$.

Three temperatures 32°C, 50°C, and 70°C, were studied. Pressure data were recorded at the set test temperature within a $\pm 0.05^\circ\text{C}$ range and later temperature corrected to the exact set temperature based on vapour pressure of water (Lide 2008).

Table 4: Saturated salt solutions for humidity control

Saturated salt solution	30 °C	50 °C	70 °C
KNO ₃	-	85.0 % RH	-
NaCl	75.1 % RH	74.5 % RH	74.1 % RH
NaCl + KCl*	71.0 % RH	-	-
KI	67.9 % RH	-	-
NaBr	-	50.9 % RH	-
MgCl ₂	-	30.5 % RH	-

* Saturated NaCl and KCl solutions were prepared separately and equal amounts of the two solutions were mixed. Crystals of both NaCl and KCl were present in the mixed solution (Winston and Bates, 1960)

A hygrometer, supplied by Omega Engineering, was used to confirm the relative humidity of the different saturated salt solutions. The hygrometer, with a resolution of 0.1 % RH, has a reported accuracy of +/- 2%RH in the range of 0 – 90% RH or +/- 3% RH at higher humidity (90-100% RH).



Figure 2 a: Wire bundles in the glass cell

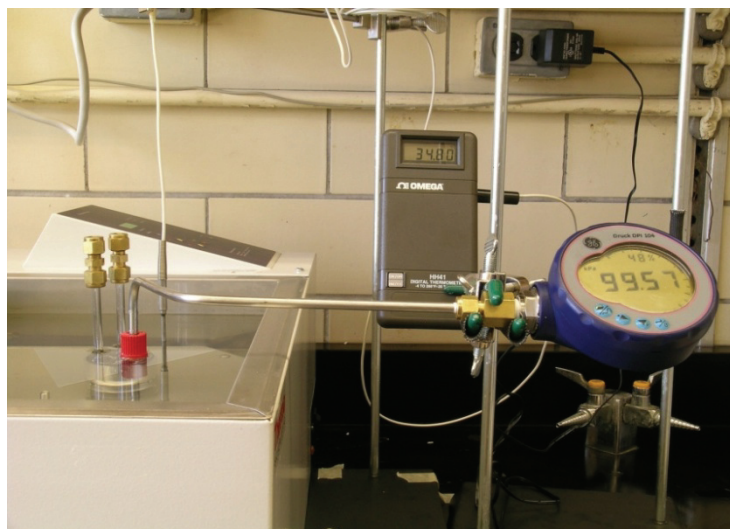


Figure 2 b: Glass cell - pressure gauge setup

2.4.1 Experimental Procedure – Pressure Gauge System

The test conditions studied in the series of corrosion experiments are tabulated in Table 1. The procedure for setting up and running the experiments was as follows:

1. Prepare test specimens by cleaning and pickling or NaCl depositing as required by the test conditions.
2. Assemble the components of the test cell in the open atmosphere.
3. Place a saturated salt solution (for humidity control) into the lower compartment of the cell with plenty of excess crystals; mount the test specimens on top of the PTFE screen inside the cell.
4. Deaerate the saturated salt solution by purging with high purity nitrogen for 2½ hours.
5. Continue deaeration of the remaining volume of the cell for another 30 minutes.
6. Close Openings 1 and 2 with rubber sheet and seal with Dow Corning high vacuum grease.
7. Close Opening 3 with a rubber ring and PTFE tape and seal with Dow Corning high vacuum grease.
8. Place the assembled test cell in the water bath to increase its temperature to the desired level.
9. Monitor pressure and temperature of the test cell. The maximum pressure allowed within the test cell was restricted to 110 kPa by pressure relief. The 110 kPa pressure level was chosen based on a leak test which had confirmed that the test cell was leak-tight with an internal hydrogen pressure of 110 kPa.
10. At the end of an experiment, dismantle the cell, measure the accumulated hydrogen concentration with the electrochemical sensor where necessary, and examine the specimens to determine the characteristics of any corrosion products.

2.4.2 Leak Test

Several leak tests were carried out to evaluate possible H₂ leakage, or losses due to H₂ adsorption on components of the test setup, or diffusion into the humidity controlling solution. Results showing the leak tightness of the glass cell and the procedure of the leak test are presented in Appendix A.

Figure 3 shows the result of one of the leak tests confirming the glass cell is air-leak tight and able to maintain a stable pressure for more than a month.

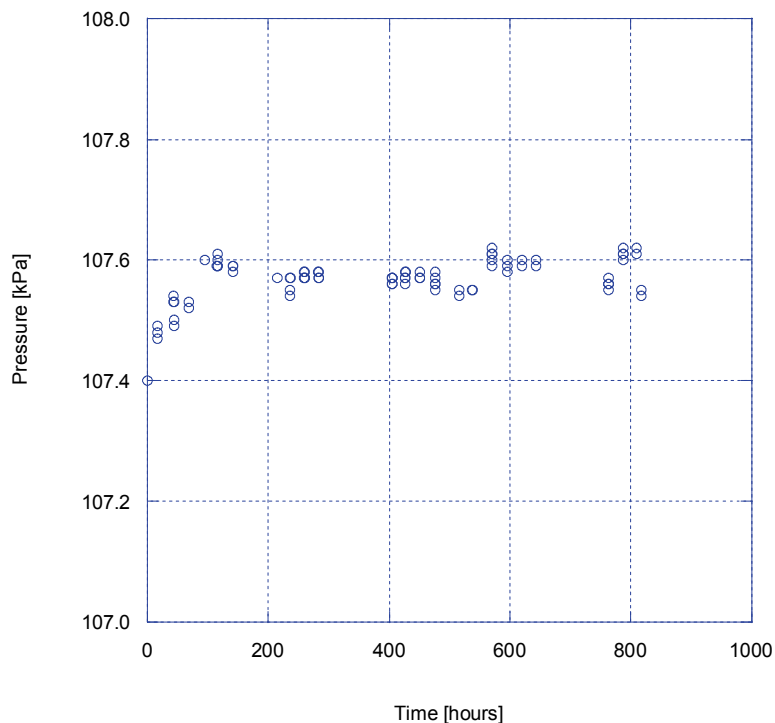


Figure 3: Typical leak test results

The outcome of the leak testing, calibration and initial corrosion testing was a good degree of confidence that the glass cell – pressure gauge system could detect meaningful temperature-corrected pressure changes down to 0.1 kPa, and perhaps less, in tests lasting hundreds of hours. The real limits of the system became evident in the less aggressive environmental conditions. The incremental depth of corrosion corresponding to a pressure change of 0.1 kPa in a cell volume of 170 mL is estimated to be ~ 0.53 nm as shown in Appendix B. This confirms that we have almost monolayer resolution on the amount of iron corroded over periods of hundreds of hours, even with a simple pressure gauge system.

2.5 Measurements of Low Rates of Hydrogen Generation Using a Solid-State Electrochemical Hydrogen Sensor in a Copper Corrosion Chamber

Since about 1983, a technology has existed for hydrogen monitoring in the gas phase, using a solid-state sensor containing a ceramic proton-conducting electrolyte (protic salt), of which the prototype was hydrogen uranyl phosphate (HUP) (Lyon and Fray, 1983). Originally the inventors and others were excited by the extraordinary sensitivity of this device, which can operate as a Nernstian potentiometric sensor and detect hydrogen partial pressures down to the 10⁻⁶ bar range. But this

mode was never very successful, and recently similar probes have been marketed that operate as unpowered amperometric sensors (like miniature fuel cells) in a more restricted range of p_{H_2} that is of interest to the oil and gas industry. A new ceramic electrolyte is used in the new probes, which does not suffer from problems with the HUP involving its oxidizing nature.

The hydrogen probe used in this study was manufactured by Ion Science Ltd, model Hydrosteel 6000. The probe operates by drawing a stream of ambient air at quite a high rate (30 ± 1 mL/min) past the electrochemical sensor. The test-gas stream is confined within a specially designed collector plate contained in the probe assembly. The collected hydrogen is conveyed through narrow bore tubing into the measurement analyzer, and across the face of a very sensitive amperometric detector. This suction approach removes the necessity for tight sealing around any barnacle type of attachment on a pipe or vessel, which is a huge advantage in practice despite the dilution of the effusing hydrogen.

For the less aggressive environments used in the pressure-gauge study, corrosion was undetectable, or became so after some time of exposure. In such cases the hydrogen sensor was used to obtain the necessary sensitivity. It was initially thought that such measurements could be made in a semi-continuous manner, by using a copper cell and effusing the produced hydrogen through a palladium membrane; alternatively a variety of approaches could be used to obtain integral hydrogen production at low levels using the sensor.

The original purpose of the copper chamber was to allow effusion of hydrogen through a palladium membrane, accumulating it in a second chamber where its concentration could be measured in a semi-continuous way by the solid-state hydrogen sensor. But after extensive studies it was concluded that this effusion method did not work. It is true that the use of palladium in such applications is rare at near-ambient temperatures. But there is no theoretical objection to the method on grounds of permeability of palladium to hydrogen; the difficulties that we experienced have to do with surface poisoning of hydrogen entry into, and exit from, the palladium membrane (Lewis, 1967). Appendix D lists the conditions attempted. We have not given up on this method, and it can be further developed in future projects.

Instead of the semi-continuous monitoring of hydrogen effusion, the hydrogen sensor was used in a batch mode to monitor cells in which the wires were corroding too slowly for any meaningful signal to be detected by pressure increase. The test conditions evaluated in this series of experiments are summarized in Table 5.

Table 5: Test conditions evaluated in the copper cell - H₂ sensor arrangement
(see also Appendix D)

Test Condition	Duration (hrs)
Pickled wires, 85% RH, 50°C	1826
Pickled wires, 75% RH, 50°C	2733
Pickled wires, 100% RH, 50°C	779

2.5.1 Experimental Procedure – H₂ sensor

The procedure for carrying out the H₂ measurements was as follows:

1. Clean all components of the copper cell with acetone and rinse thoroughly with de-ionized water.
2. Assemble the internal components of the copper cell by placing a PTFE plate in a 50 mL beaker and putting the 50 mL beaker into a 100 mL beaker. The PTFE plate is provided to drain off condensation from the wire surfaces. Put both beakers into the copper cell (Figure 5).
3. Deaerate 20 mL of saturated salt solution with N₂ for 2 hours and pour the deaerated salt solution into the 100 mL beaker (inside the copper cell).
4. Prepare the test wires by cleaning and pickling as required by the test conditions.
5. Place the prepared wire bundles into the 50 mL beaker, on top of the PTFE screen (Figure 4).
6. Continue deaeration for another 30 minutes before closing the valve of the cell and sealing the cell using PTFE tape and vacuum grease.
7. Place the copper cell into the water bath at a pre-set temperature.
8. In initial trials where a palladium membrane was used (Figure 6), the palladium foil was pretreated separately. Various pre-treatment conditions were tried, including (i) heating the foil in an oven at 720-900°C for 30 – 60 minutes, then at 500 °C for another 30 minutes; (ii) reducing any surface oxide on the Pd surface by flushing the foil with Ar + 2.5% H₂ mixture in a tube furnace for 5 minutes at 200°C; (iii) coating the Pd foil exit surface with 0.1M NaOH. After the pretreatment, the Pd foil was mounted between the upper and lower compartments of the copper cell and a mixture of N₂ and 100 ppm H₂ was then introduced into the copper cell for 30 minutes. The valve of the cell was then closed and the copper cell was sealed with PTFE tape and vacuum grease. H₂ measurements were carried out at various time intervals using the H₂ probe but none of these pre-treatments were found effective in resolving the surface poisoning problem encountered on the palladium membrane.
9. The procedure for monitoring H₂ in a batch mode is as follows:
 - a) Prepare the test wires and assemble the copper cell as described above.
 - b) At various time intervals (typically about 8-10 days), measure the accumulated H₂ in the copper cell by placing it into a glove box, along with the hydrogen sensor and other accessories required for H₂ measurement (e.g.. thermometer and pressure gauge).
 - c) Deaerate the glove box with high purity nitrogen gas for 1 hour.
 - d) Seal the glove box, then record the temperature and pressure of both the copper cell and the glove box.
 - e) Connect the H₂ probe to the copper cell valve and begin H₂ recording until H₂ detection is complete. Disconnect the H₂ probe from the copper cell.
 - f) Unseal the glove box and repeat deaeration of the glove box with N₂ for 1 hour.
 - g) Reseal the glove box, close the copper cell valve.
 - h) Return the copper cell to the water bath until the next measurement.



Figure 4: Prepared wires in beaker, on top of PTFE



Figure 5: Prepared wires in beaker, placed in the copper cell



Figure 6 a: Upper compartment of the copper cell without the palladium membrane



Figure 6 b: Upper compartment of the copper cell with the palladium membrane mounted

2.5.2 H₂ Sensor Calibration Procedure

Prior to its use, the hydrogen sensor was calibrated with 97 ppm hydrogen gas (balanced with N₂) as follows:

1. Assemble the copper cell as described in Section 2.5.1.
2. Place the copper cell (cell valve opened), H₂ probe and other measurement accessories in the glove box.
3. Deaerate the glove box with N₂ for 1 hour, follow by another hour of N₂ / H₂ flushing (97 ppm H₂).
4. Close the copper cell valve and record the temperature and gas pressure of the glove box.
5. Release H₂ from the glove box.
6. Connect the H₂ probe to the copper cell valve and begin H₂ measurement by opening the copper cell valve.
7. The calibration results are presented in Appendix D.
8. The maximum probe reading is used to determine the hydrogen concentration accumulated in the copper cell.

2.5.3 H₂ Measurement - Pressure Gauge System

The concentration of H₂ accumulated in the glass cell was measured on a few occasions in a similar manner as in the copper cell setting.

2.6 Analysis of Corrosion Products

2.6.1 Surface Analysis and Microscopy

The following surface analytical measurements were carried out at Surface Science Western, University of Western Ontario, to determine the surface oxide morphology, composition and where possible, chemical state, as a result of exposure to various environmental conditions:

1. Preliminary optical microscopy examinations were performed using a low power (10X – 80X) Zeiss Discovery V8 stereozoom microscope and a high power Zeiss Axioplan optical microscope.
2. Scanning Electron Microscopy coupled with Energy Dispersive X-ray Analysis (SEM/EDX) was performed using a Leo 440 conventional SEM equipped with a Quartz Xone EDX system. Secondary electron micrographs and EDX spectra were obtained from two different areas of interest per sample.
3. X-ray Photoelectron Spectroscopy (XPS) analyses were performed using a Kratos AXIS Ultra X-ray photoelectron spectrometer. Monochromatic X-rays produced by an Al ($K\alpha$) source were bombarded on the specimen and the resulting photoelectrons were collected using a spherical mirror analyser. Survey scan spectra were collected from an analysis area of 300 x 700 microns with a pass energy of 160 eV. High resolution XPS analyses were carried out on an analysis area of 300 x 700 microns with a pass energy of 20 eV.
4. Laser Raman Spectroscopy measurements were performed using a Renishaw Model 2000 Raman Spectrometer. The measurements were made using a 633 nm laser. The sampling area for this analysis is approximately 2 μm in diameter.
5. Finally Fourier Transform Infrared Spectroscopy (FTIR) was performed to give further information on bonding. FTIR measurements were performed using a Bruker IFS55 instrument under reflection mode using a microscope attachment.

2.6.1.1 X-ray Photoelectron Spectroscopy

Steel specimens, following exposures to various humidity and temperature conditions, were sealed in NMR glass tubes under anaerobic conditions and transferred to Surface Science Western (SSW) for surface analytical examination.

To begin the analysis, the NMR tube containing the steel specimens was placed in a glove box attached to the XPS instrument. The glove box was deaerated by purging with high purity dry argon gas for 1.5 to 2 hours. The NMR tube was then broken open and the steel wires were removed from the NMR tubing under the anoxic conditions. Small representative sections of the wire were then cut and placed on a XPS sample holder. Due to the small diameter of the steel wires (0.25 mm), the cut wire segments were placed across an opening in the holder so that the background of the sample holder was not analyzed. The sample holder was then transferred into the XPS instrument under vacuum for XPS survey scans, and high-resolution spectra were collected from selected locations of interest.

As wet-oxidized steel surfaces are expected to be highly oxygen-sensitive, it was expected that some traces of Fe III oxide or oxyhydroxide might be found even after these precautions, and indeed this was the case.

2.6.1.2 Scanning electron microscopy

After XPS analysis, wire samples were removed from the sample holder and transferred to the SEM chamber as quickly as possible in order to minimize air exposure. After SEM/EDX analysis, the wire samples were stored in a vacuum desiccator until other surface analyses were available.

2.6.1.3 Raman spectroscopy

Bonding information on the corrosion products formed on the steel wires was determined using Raman spectroscopy, an optical technique with which chemical and phase-specific information can be obtained non-destructively. Several procedures were assessed. Initial Raman measurements were conducted on the steel wire samples inside their NMR tubes. The wires sat at the bottom of the tube which increased the distance between the objective lens and the steel wire surface. This resulted in exceptionally long acquisition times with very weak Raman response. To attempt to resolve this problem, the steel wire sample was bent prior to encapsulation into the NMR tube so that a portion of the wire surface was closer to the wall of the NMR tube and hence to the objective lens. This procedure did not provide satisfactory improvement of the signal intensity. Finally, comparative Raman measurements were performed on steel wire samples in the as-encapsulated condition and on the wire surface removed from the NMR tubing. The positions of features on Raman spectra from both measurements were comparable and brief exposure to the atmosphere did not seem to cause any significant differences.

2.6.1.4 Fourier Transform Infrared Spectroscopy (FTIR)

In addition to the specific vibrational information of the iron oxides present on the wire surface obtained in the Raman spectroscopy, FTIR was performed to provide further characterization information of the formed oxides. To minimize air exposure, FTIR measurements were performed immediately after Raman imaging.

2.7 Quartz Crystal Microbalance (QCM)

The quartz crystal microbalance has been used to quantify mass gain or loss resulting from dissolution or thin-film growth in metal corrosion studies. The QCM is based on the principle that when the mass of a vibrating cantilever changes, so does its frequency of vibration (Sullivan and Guilbault, 1999; Henry, 1996). In electrochemistry and vacuum technology, it is well recognized that the QCM has sub-monolayer sensitivity, and at the outset of this project we believed it had very good potential for measuring the kinetics of iron oxidation. This turned out not to be the case, and the reasons are provided in Appendix C.

3. RESULTS

3.1 Glass Cell – Pressure Gauge Experiments

All the glass-cell testing has been graphed as raw, temperature-corrected pressure data and as “corrosion rates” derived from differentiation of those data. In tests showing high corrosion rates, the raw data show discontinuities due to occasional pressure relief.

Earlier we mentioned that a measurable pressure increase of 0.1 kPa corresponded, with our standard testing conditions such as metal surface area to 0.53 nm of corroded iron, assuming that the corrosion product is $\text{Fe}(\text{OH})_2$ (the calculation is shown in Appendix B). So a corrosion rate of $1 \mu\text{m}\cdot\text{y}^{-1}$ would correspond to $189 \text{ kPa}\cdot\text{y}^{-1}$, or $0.022 \text{ kPa}\cdot\text{h}^{-1}$. Such corrosion rates can be easily monitored daily. On the other hand, a corrosion rate of $0.01 \mu\text{m}\cdot\text{y}^{-1}$ corresponds to $0.005 \text{ kPa}\cdot\text{d}^{-1}$. In that case, some weeks might be required to track a corrosion rate reliably. Table 6 summarizes the results obtained from the glass cell-pressure gauge experiments.

3.1.1 NaCl dipped wires

Corrosion rates in tests where the wire samples were coated with NaCl by soaking in 0.05 M and 0.5M NaCl solutions and drying, then exposed to various relative humidities and temperatures. The estimated corrosion rates and kinetic data are shown in Figures 7 to 18. The estimated corrosion rates at the end of the tests were found to be in the range of 0.01 to $0.8 \mu\text{m}\cdot\text{y}^{-1}$ for test durations of 935 to 1725 hours. Higher transient corrosion rates in the range of 1 to $5 \mu\text{m}\cdot\text{y}^{-1}$ were found for tests with shorter test durations of 213 to 450 hours.

At 32°C , the final corrosion rates were estimated to be about 0.15 to $0.45 \mu\text{m}\cdot\text{y}^{-1}$ for RH in the range of 68% to 100% (Table 6). The corrosion rates appear to be slightly higher at lower (68 to 75%) RH than at 100% RH (Figure 19), which may be explained by a more concentrated thin-film electrolyte at lower RH. This was, however, not a general result, as testing at 50°C showed the reverse trend.

Table 6: Glass cell - pressure gauge experimental results

Test Conditions	Duration	Estimated Corrosion Rate (final)
0.5M NaCl dipped wires		
▪ 68% RH, 32°C	1347 hrs	< 0.15 $\mu\text{m}\cdot\text{y}^{-1}$
▪ 71% RH, 32°C	935 hrs	~ 0.2 $\mu\text{m}\cdot\text{y}^{-1}$
▪ 75% RH, 32°C	1730 hrs	< 0.4 $\mu\text{m}\cdot\text{y}^{-1}$
▪ 100% RH, 32°C	1269 hrs	< 0.4 $\mu\text{m}\cdot\text{y}^{-1}$
▪ 30.5% RH, 50°C	1962 hrs	< 0.01 $\mu\text{m}\cdot\text{y}^{-1}$
▪ 51% RH, 50°C	1053 hrs	< 0.01 $\mu\text{m}\cdot\text{y}^{-1}$
▪ 75% RH, 50°C	450 hrs	< 1 $\mu\text{m}\cdot\text{y}^{-1}$
▪ 100% RH, 50°C	237 hrs	< 3 $\mu\text{m}\cdot\text{y}^{-1}$
▪ 100% RH, 50°C (II)	1725 hrs	0.8 $\mu\text{m}\cdot\text{y}^{-1}$
▪ 100% RH, 70°C	213 hrs	< 5 $\mu\text{m}\cdot\text{y}^{-1}$
0.05M NaCl dipped wires		
▪ 51% RH, 50°C	1867 hrs	< 0.01 $\mu\text{m}\cdot\text{y}^{-1}$
▪ 75% RH, 50°C	2326 hrs	~ 0.08 $\mu\text{m}\cdot\text{y}^{-1}$
▪ 75% RH, 32°C	3355 hrs	< 0.01 $\mu\text{m}\cdot\text{y}^{-1}$
Degreased wires		
▪ 100% RH, 32°C	379 hrs	< 0.001 $\mu\text{m}\cdot\text{y}^{-1}$
▪ 100% RH, 50°C (deaerated with N ₂)	615 hrs	< 0.001 $\mu\text{m}\cdot\text{y}^{-1}$
▪ 100% RH, 50°C (deaerated with N ₂ & H ₂)	591 hrs	< 0.001 $\mu\text{m}\cdot\text{y}^{-1}$
Pickled wires		
▪ 75% RH, 32°C	1171 hrs	---
▪ 100% RH, 32°C	1337 hrs	< 0.001 $\mu\text{m}\cdot\text{y}^{-1}$
▪ 75% RH, 50°C	331 hrs	< 0.001 $\mu\text{m}\cdot\text{y}^{-1}$
▪ 100% RH, 50°C	1002 hrs	< 0.01 $\mu\text{m}\cdot\text{y}^{-1}$
▪ 100% RH, 50°C (reused wires from 75% RH)	688 hrs	< 0.01 $\mu\text{m}\cdot\text{y}^{-1}$
▪ 74.1% RH, 70°C	1121 hrs	< 0.01 $\mu\text{m}\cdot\text{y}^{-1}$
▪ 100% RH, 70°C	1006 hrs	< 0.01 $\mu\text{m}\cdot\text{y}^{-1}$

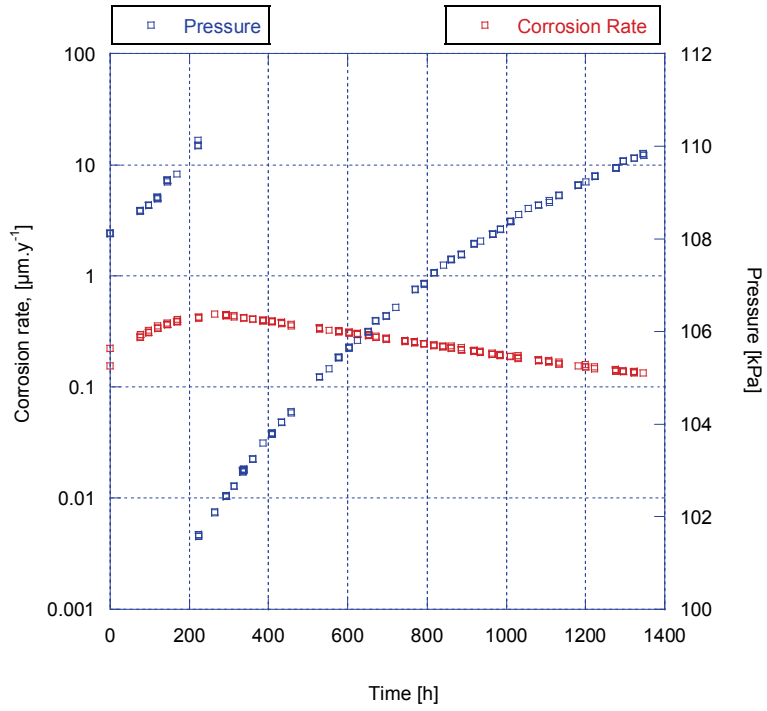


Figure 7: Corrosion behaviour of 0.5M NaCl dipped wires tested at 32°C and 68% RH

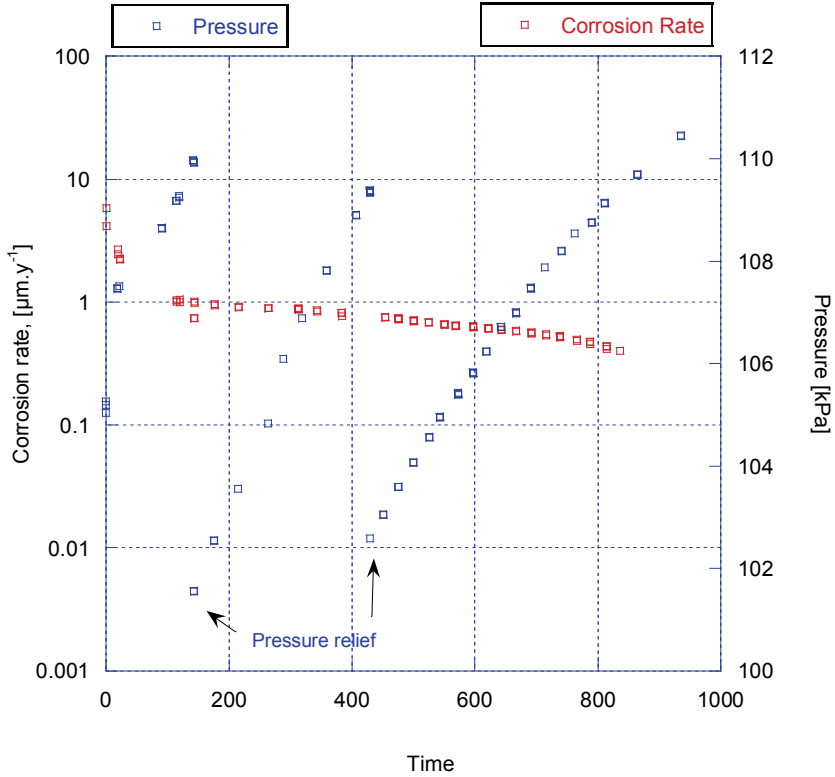


Figure 8: Corrosion behaviour of 0.5M NaCl dipped wires tested at 32°C and 71% RH

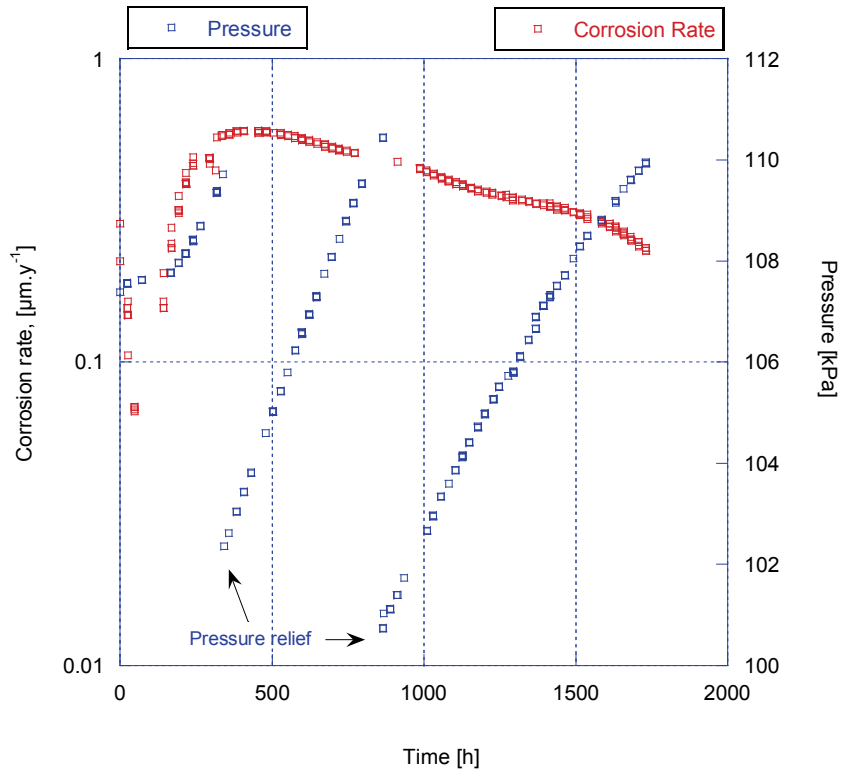


Figure 9: Corrosion behaviour of 0.5M NaCl dipped wires tested at 32°C and 75% RH

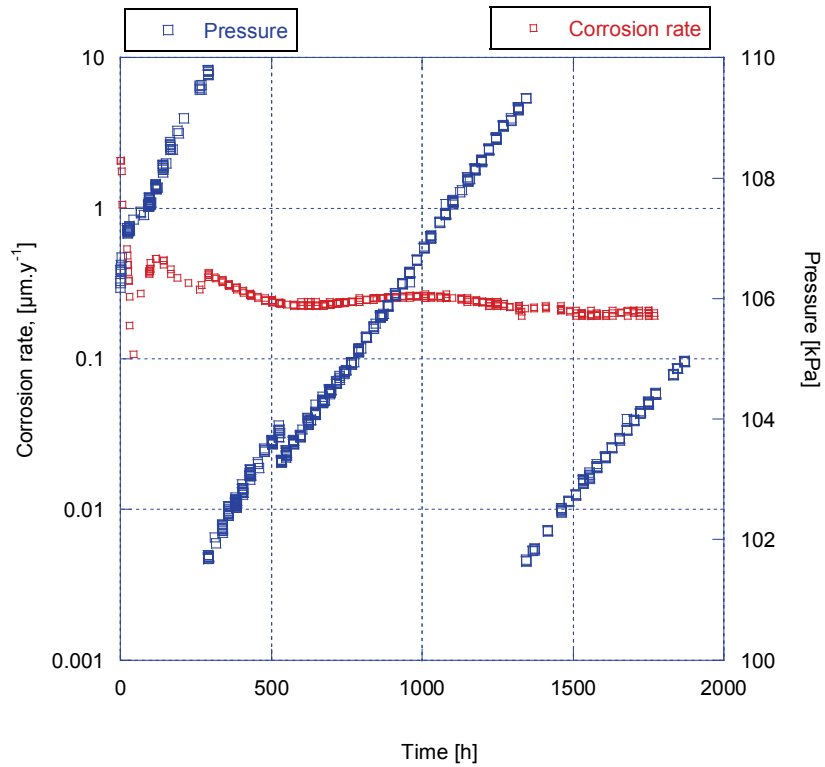


Figure 10: Corrosion behaviour of 0.5M NaCl dipped wires tested at 32°C and 100% RH

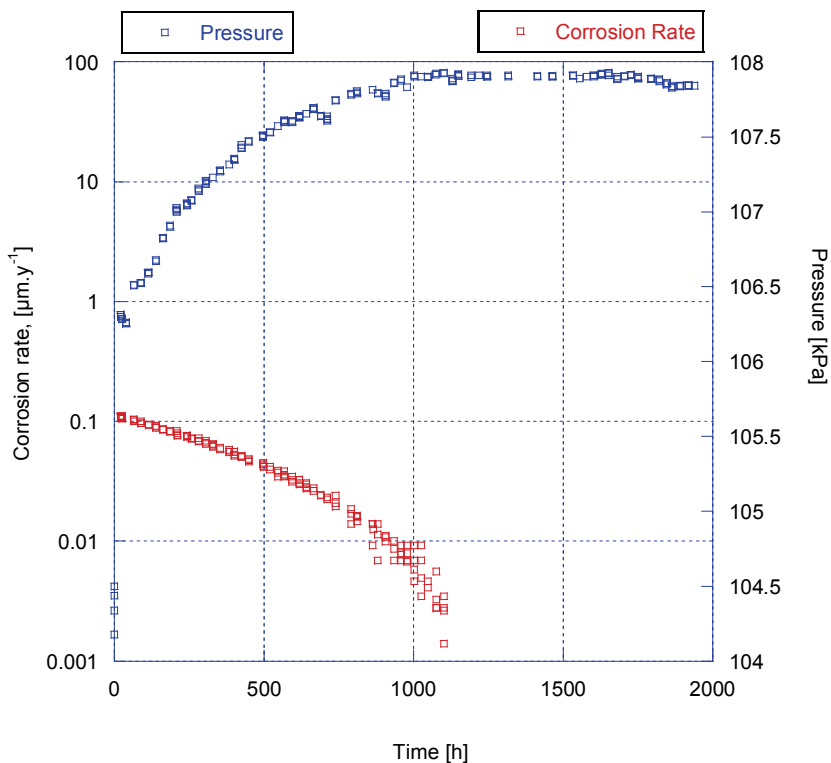


Figure 11: Corrosion behaviour of 0.5M NaCl dipped wires tested at 50°C and 30.5% RH

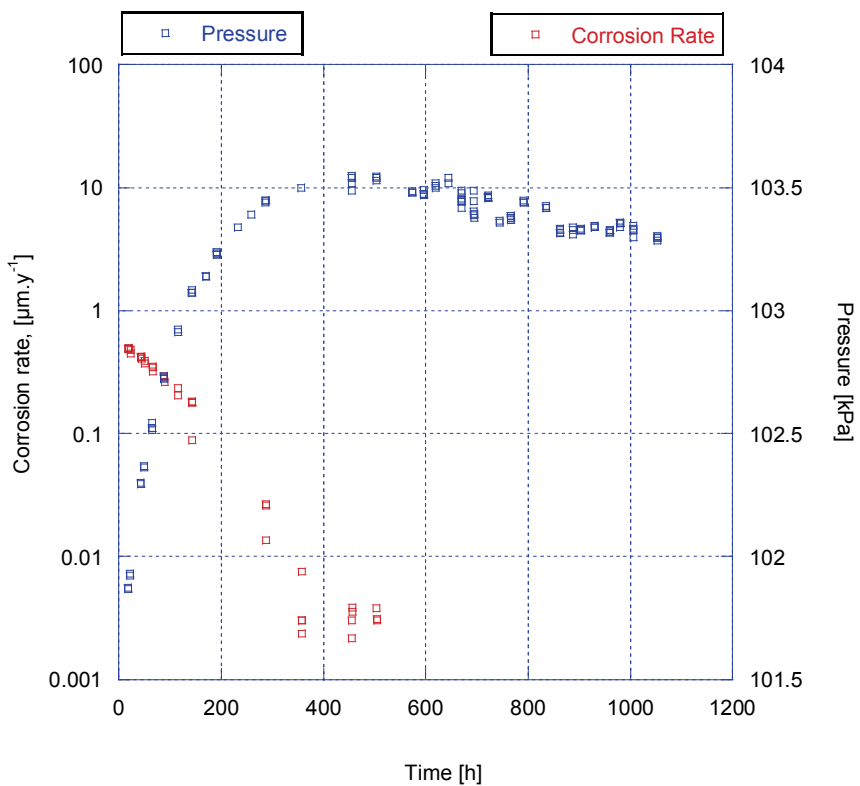


Figure 12: Corrosion behaviour of 0.5M NaCl dipped wires tested at 50°C and 51% RH

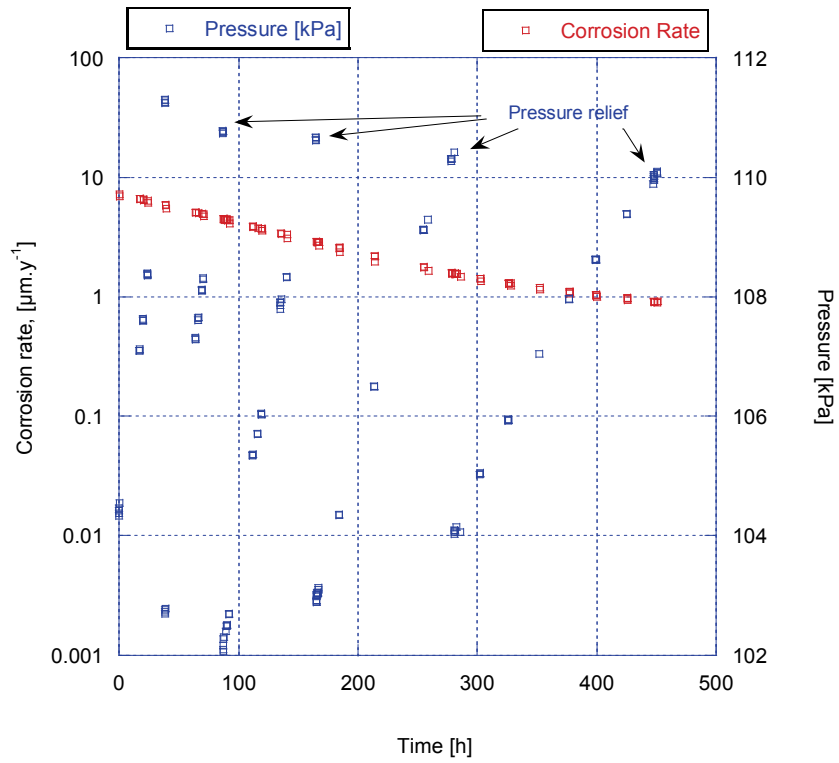


Figure 13: Corrosion behaviour of 0.5M NaCl dipped wires tested at 50°C and 75% RH

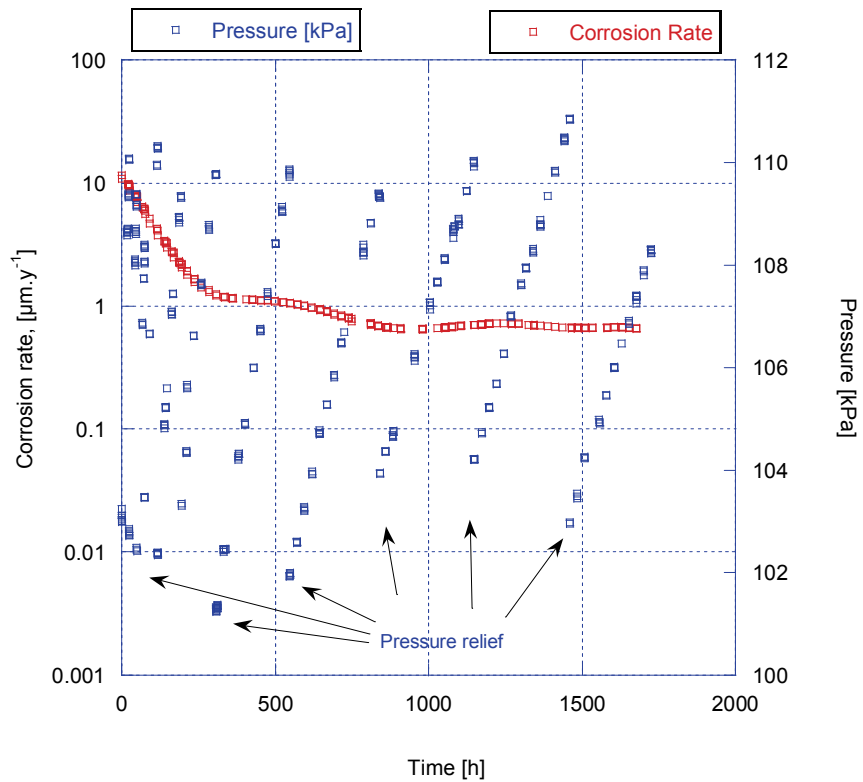


Figure 14: Corrosion behaviour of 0.5M NaCl dipped wires tested at 50°C and 100% RH

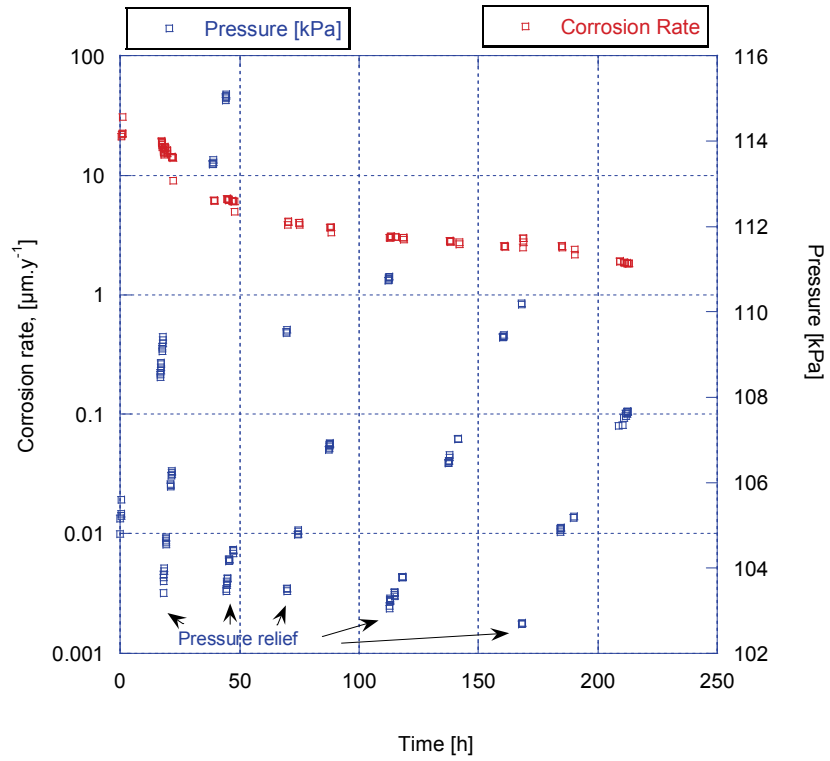


Figure 15: Corrosion behaviour of 0.5M NaCl dipped wires tested at 70°C and 100% RH

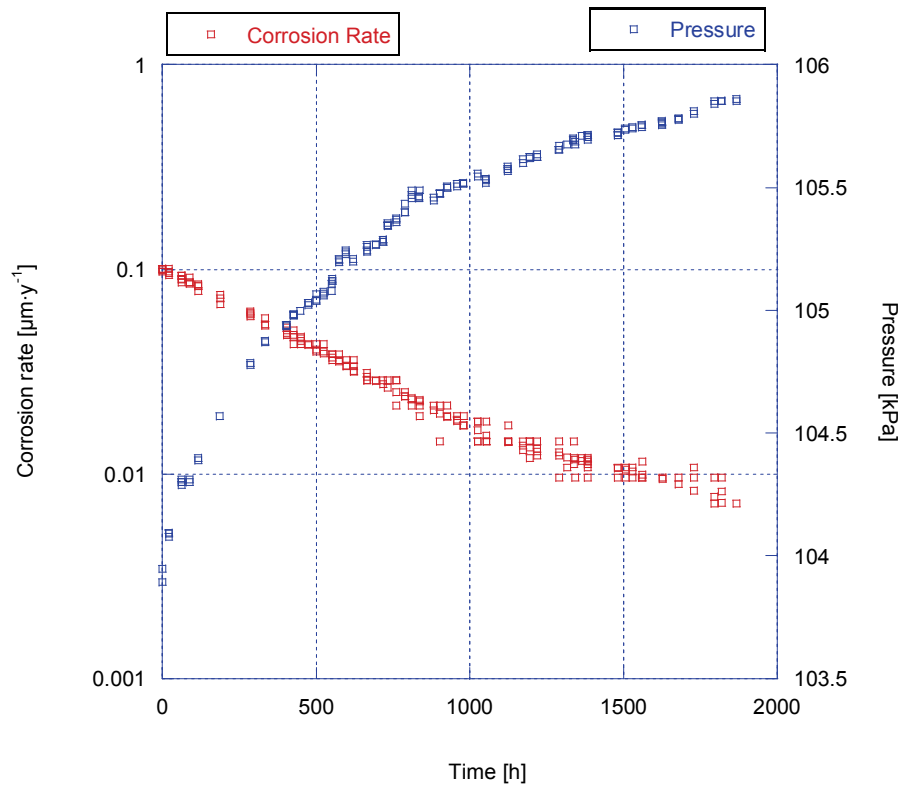


Figure 16: Corrosion behaviour of 0.05M NaCl dipped wires tested at 50°C and 51% RH

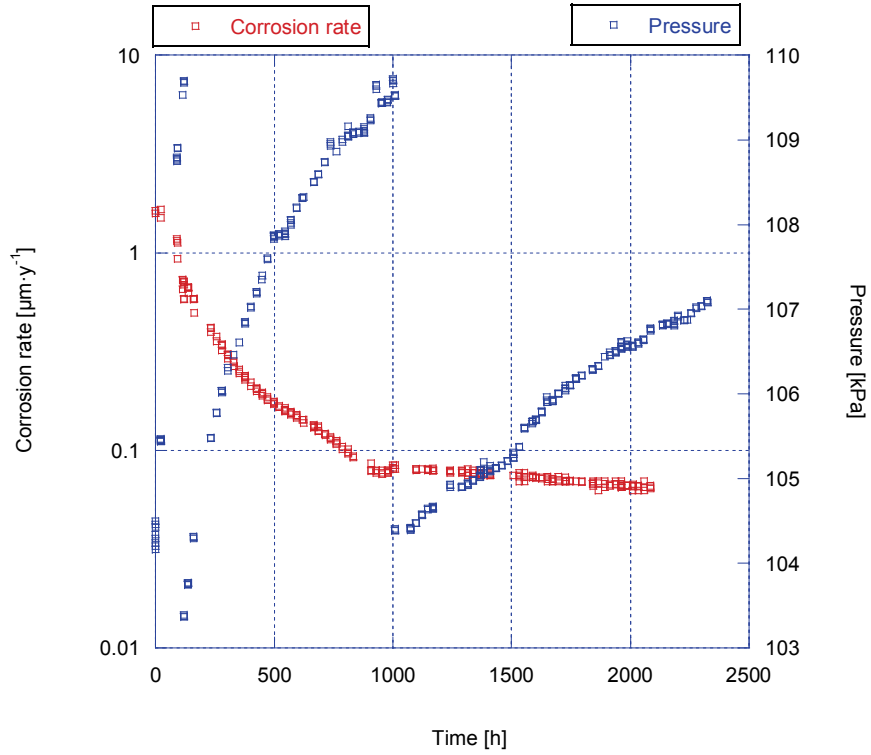


Figure 17: Corrosion behaviour of 0.05M NaCl dipped wires tested at 50°C and 75% RH

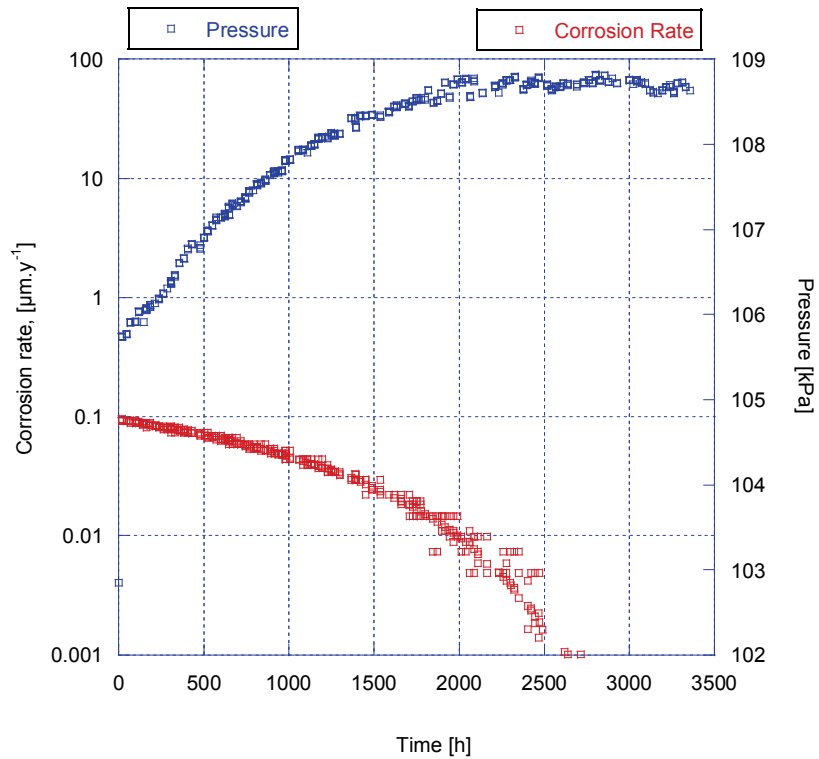


Figure 18: Corrosion behaviour of 0.05M NaCl dipped wires tested at 32°C and 75% RH

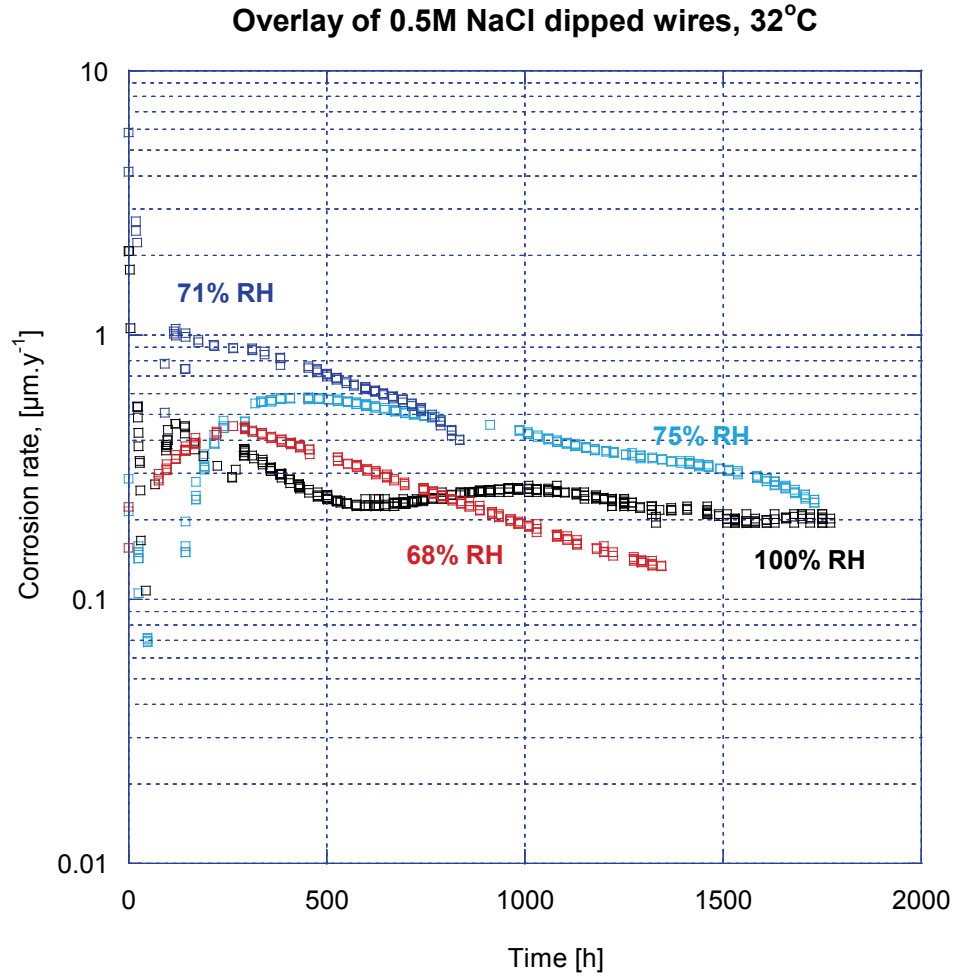


Figure 19: Corrosion behaviour of 0.5M NaCl dipped wires tested at 32°C and various RH

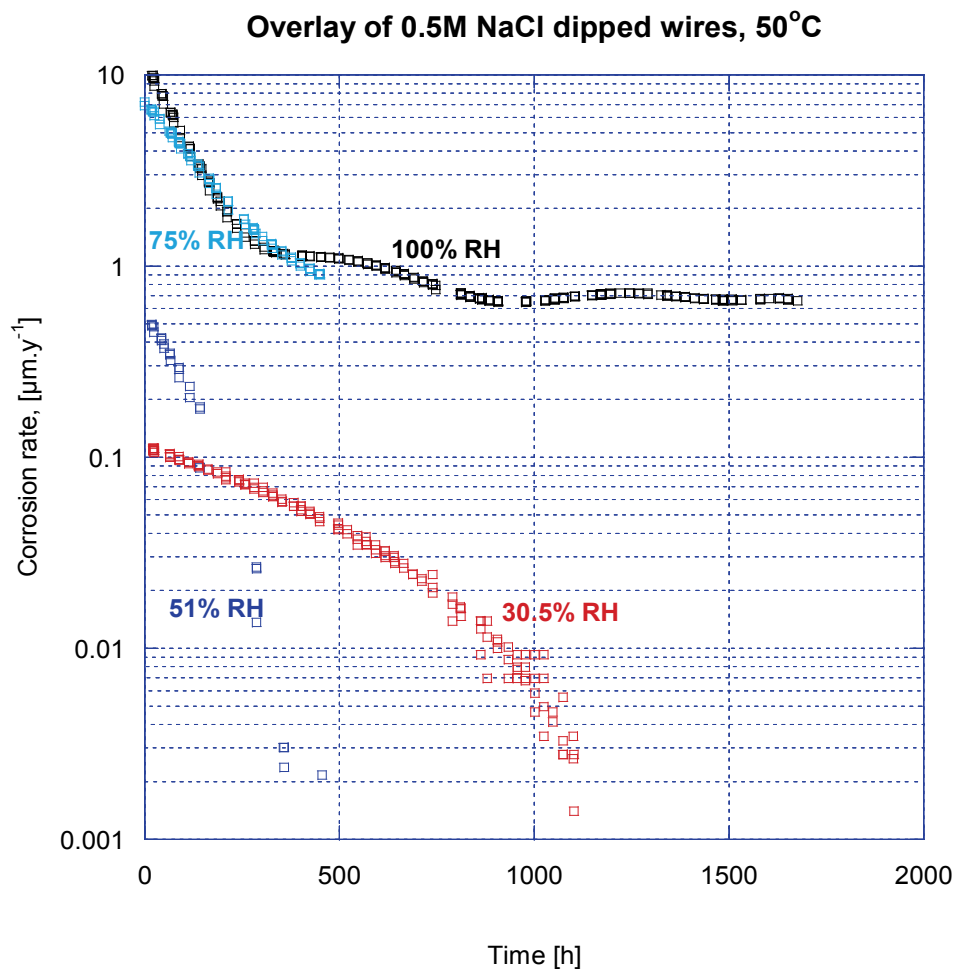


Figure 20: Corrosion behaviour of 0.5M NaCl dipped wires exposed to 50°C and various RH

At a higher temperature of 50 °C, the estimated corrosion rates were 1 and 0.8 $\mu\text{m}\cdot\text{y}^{-1}$ at 75% and 100% RH, respectively (Table 6). The test at 75% RH is still in its rapid transient stage since the test duration is short (450 hours) (Figure 20). At 30.5 and 50% RH, the estimated final corrosion rates were much lower, ca. 0.01 $\mu\text{m}\cdot\text{y}^{-1}$, which was still within the resolution range of the pressure gauge method (Table 6 and Figure 20).

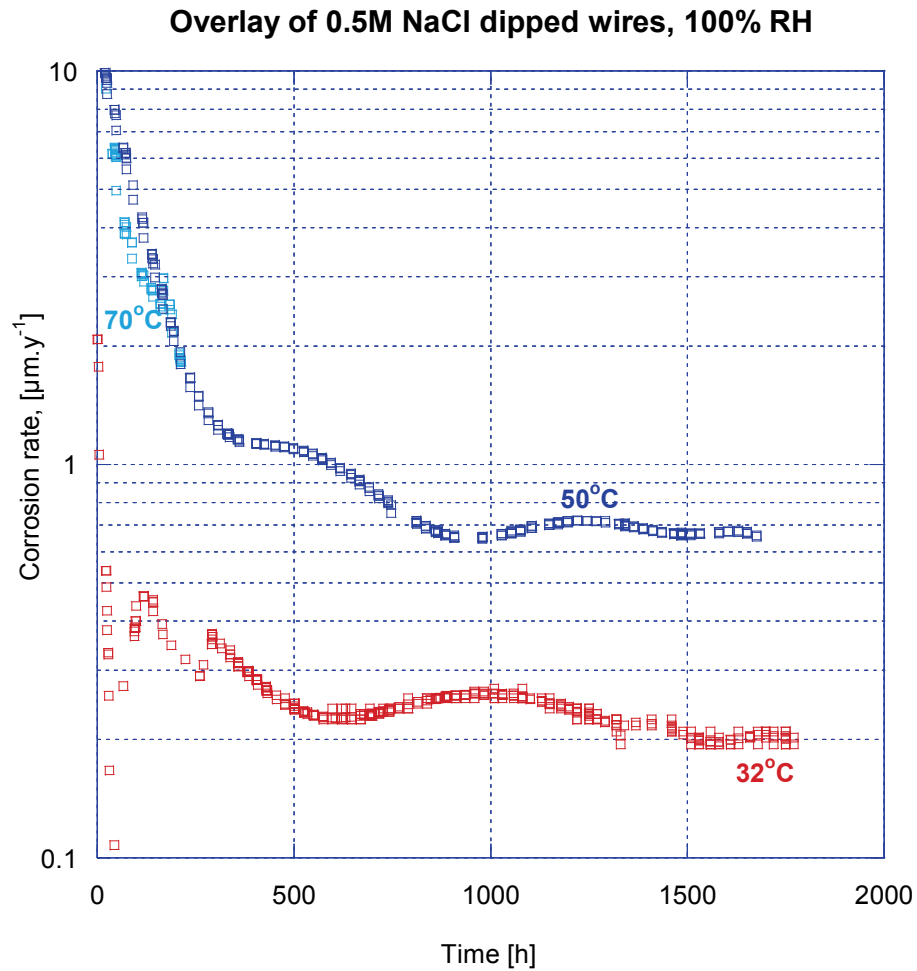


Figure 21: Corrosion behaviour of 0.5M NaCl dipped wires exposed to 100% RH and various temperatures

Interestingly, the tests at 32 °C and 75% RH indicate that soaking the wires in 0.05M NaCl solution was much less aggressive than soaking in 0.5M NaCl solution (Figure 22). With 0.05M NaCl soaking, the metal loss tended to level out with time, indicating that chloride is more than just a catalyst for corrosion – the thickness of liquid layer and absolute quantity of chloride in that layer are important. These test results appear to indicate that corrosion rates may increase quite sharply with increasing concentration of the NaCl solution and increasing amount of NaCl deposited on the wire surface.

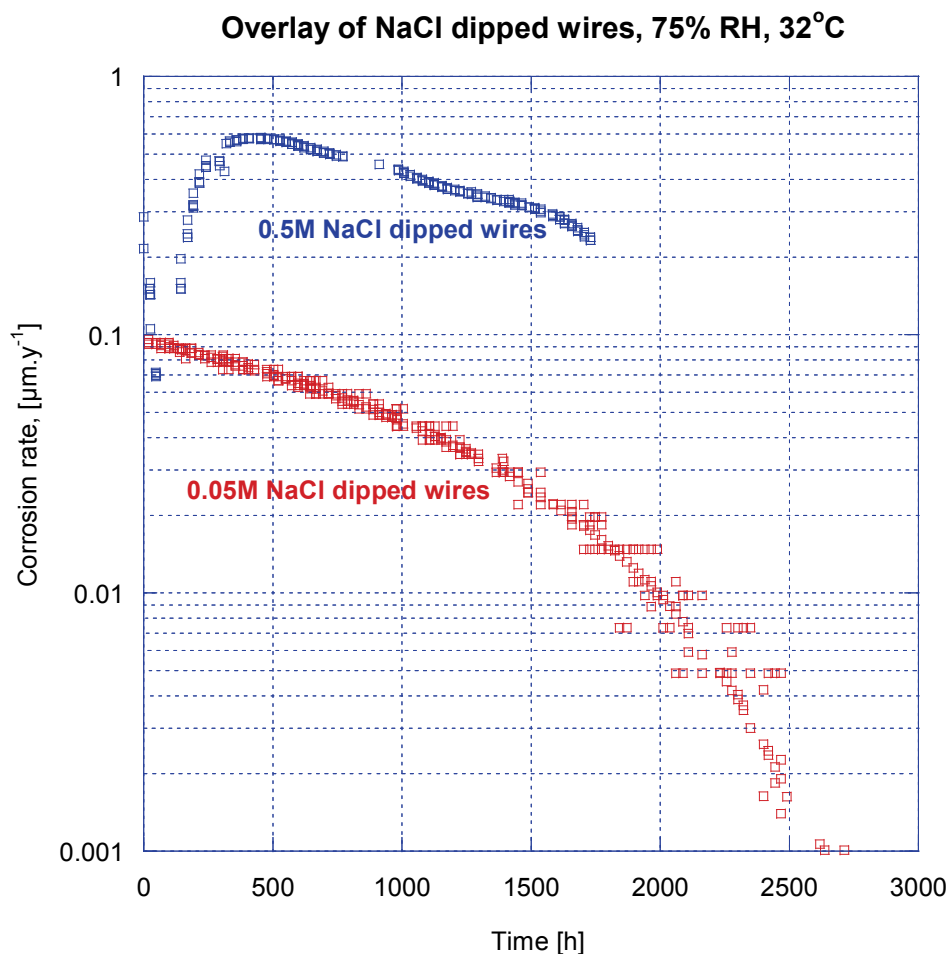


Figure 22: Corrosion behaviour of NaCl dipped wires exposed to 75% RH, 32°C

These test results appear to show that steel corrosion would not stop as the relative humidity was reduced to, or slightly below, the value that is in equilibrium with saturated NaCl (i.e. 75.5%RH at 30°C and 74.5%RH at 50°C) (Figure 23). This is a well-known finding for atmospheric corrosion in ordinary aerated environments - that 60-70% RH provides sufficient moisture to support electrochemical reactions - but this is probably the first such study in anoxic environments. Various explanations for this are possible, including simple gas-phase reaction with water vapour, reaction with multilayer adsorption of water, hydrous corrosion products, capillary condensation, and involvement of hygroscopic iron salts ($\text{FeCl}_2 \cdot x\text{H}_2\text{O}$). Nevertheless, there was a steep decline in corrosion rate as the RH was reduced to 30.5% and 51% (Figure 23). At these low RH values, corrosion is not well sustained.

Overlay of 0.5M NaCl dipped wires, exposed to various conditions

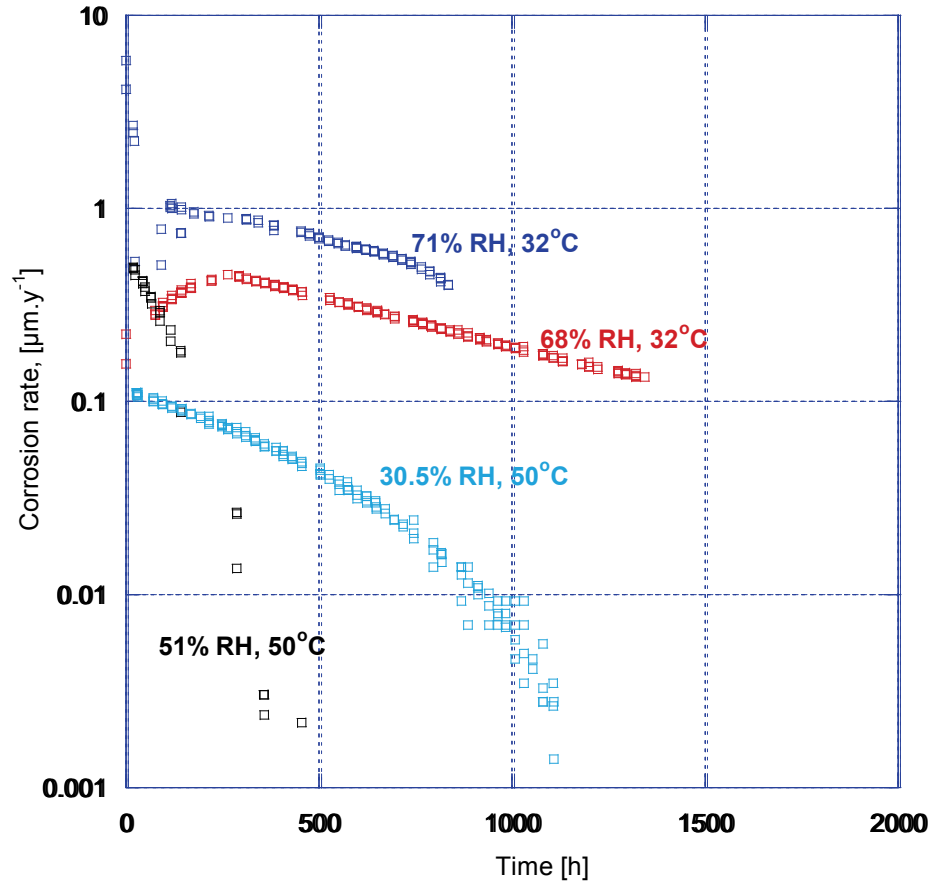


Figure 23: Corrosion behaviour of 0.5M NaCl dipped wires exposed to $\text{RH} \leq \text{equilibrium RH}$

The time dependence of corrosion rate for the tests that showed sustained corrosion in Figures 7 to 23 was not easy to fit to any rational law that might enable extrapolation to longer times. However it is evident, even from visual observation of the curves, that some corrosion rate decays approximate to exponentials with rather long time constants, e.g. the 68% RH data in Figure 23. We would not advise extrapolating such curves for predictive purposes, as we have seen both kinds of deviation – positive and negative – from such initially well-behaved lines. But just for illustrative purposes, the straight-line decay in Figure 24 approximates to the following:

$$R = R_0 \exp \frac{-t}{\tau}$$

with $R_0 \simeq 6 \mu\text{m}\cdot\text{y}^{-1}$ and $\tau \simeq 870 \text{ h}$. R , R_0 and τ are defined as corrosion rate at time t , “initial” corrosion rate (after curve fitting) and decay time constant, respectively. If we could believe in such a decay law, the corrosion rate would fall to 0.5 nm y^{-1} after only 1 year! But the rate controlling process can change with time, and the conservative way to use the data is to take the minimum observed corrosion rate and assume that it would be sustained over time.

Other curves are better fitted by power laws, leading to more pessimistic predictions for long-term corrosion rates. Figure 24 shows a reasonable $t^{-0.6}$ fit for the data of Figure 15, but this may be too conservative as the corrosion rate shows a dip towards the end of the test. But even taking the fit at face value, the corrosion rate would fall to $0.24 \mu\text{m y}^{-1}$ after 1 year, and 3.7 nm y^{-1} after 1000 years. Is it legitimate to make such extrapolations? More testing would be required to sustain the speculation that this is an upper limit on the corrosion rate because of the dip seen at the end of the limited dataset!

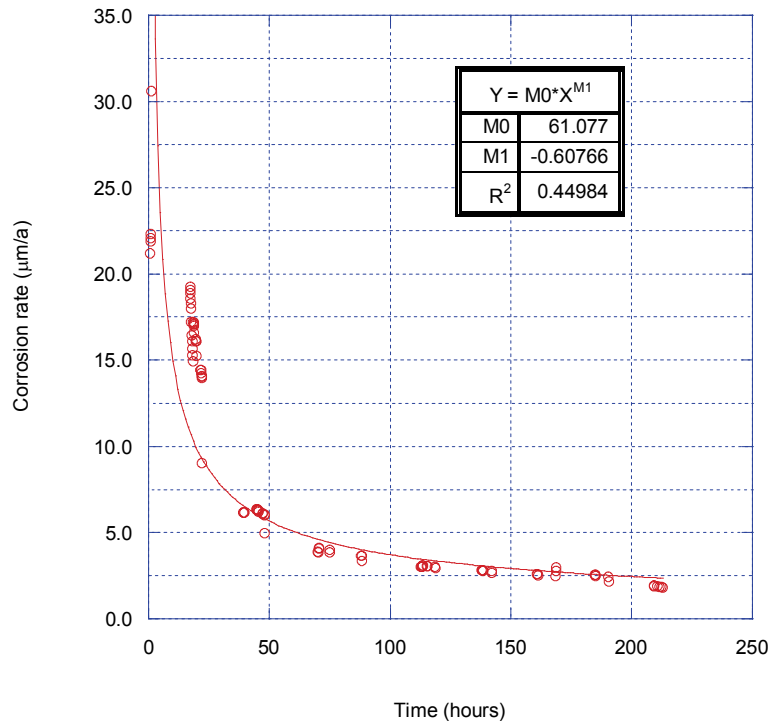


Figure 24: Power curve fit of corrosion rates - 0.5M NaCl dipped wires, exposed to 70°C and 100% RH

3.1.2 Surfaces with no salt deposit

When wires were exposed without any salt deposit, the pressure gauge method began to approach its limit of sensitivity for the detection of hydrogen, and when it did occur detectably, the hydrogen generation was mostly transient in nature. It is these tests that form the basis for the use of the hydrogen sensor in the next stage.

While similar behaviour was noticed for the pickled wires at 32, 50 and 70°C, 100% RH, none of these tests (Figures 25-28) showed any conclusive indication of long-term sustained corrosion, as the pressure changes became too difficult to detect shortly after the experiments started. A key application of the hydrogen sensor is to determine whether corrosion has really “stopped” after this sequence. [One might also ask, for the pickled-wire testing - could hydrogen be absorbed from the pickling, then effuse during the test – but if that were the case, this should happen in every test, which it did not.]

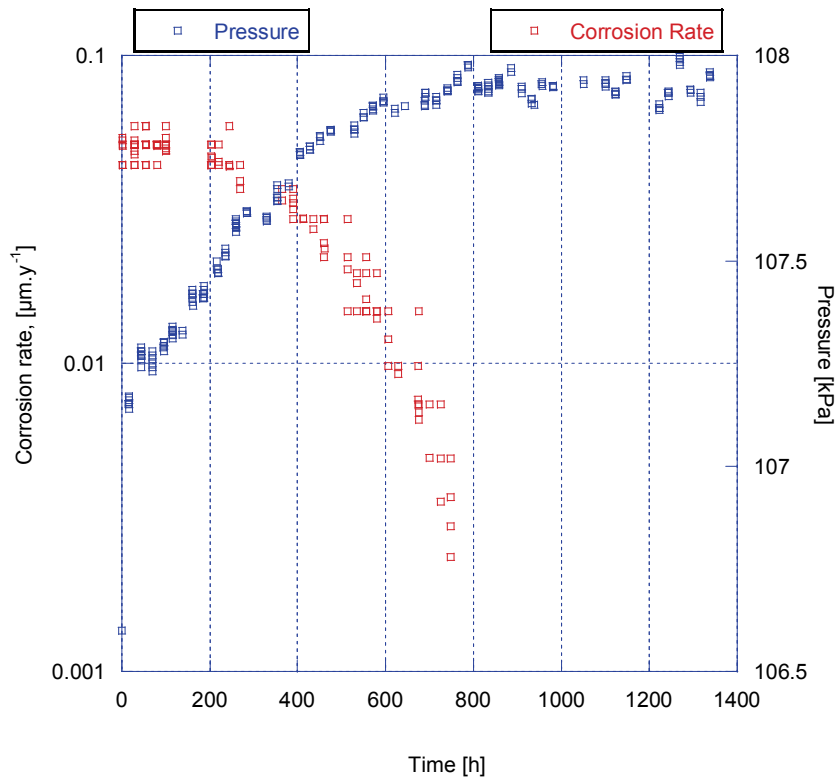


Figure 25: Corrosion behaviour of pickled wires exposed to 32°C, 100% RH

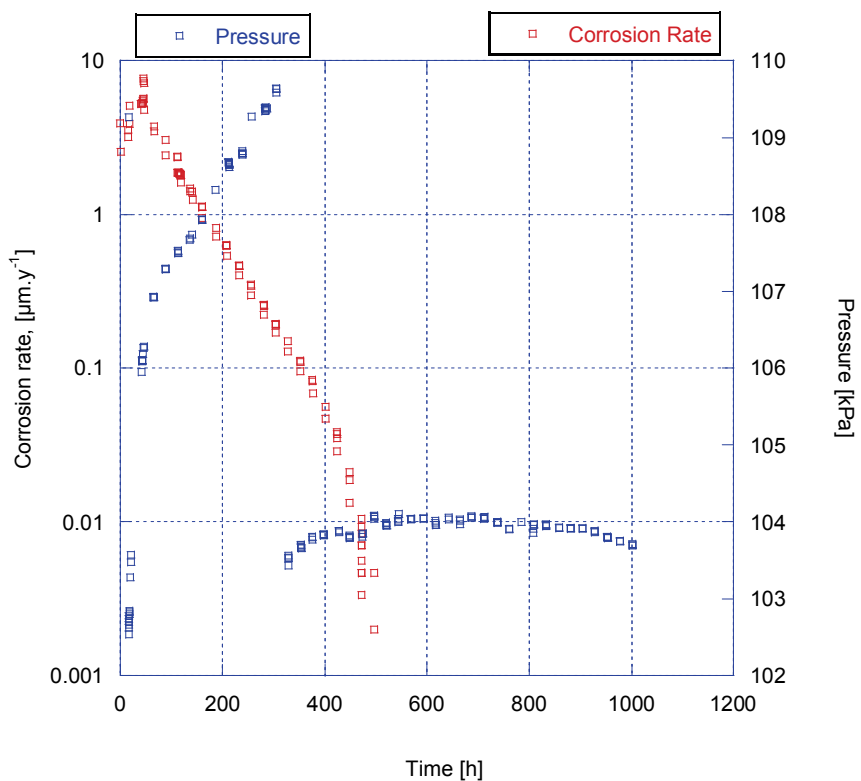


Figure 26: Corrosion behaviour of pickled wires exposed to 50°C, 100% RH

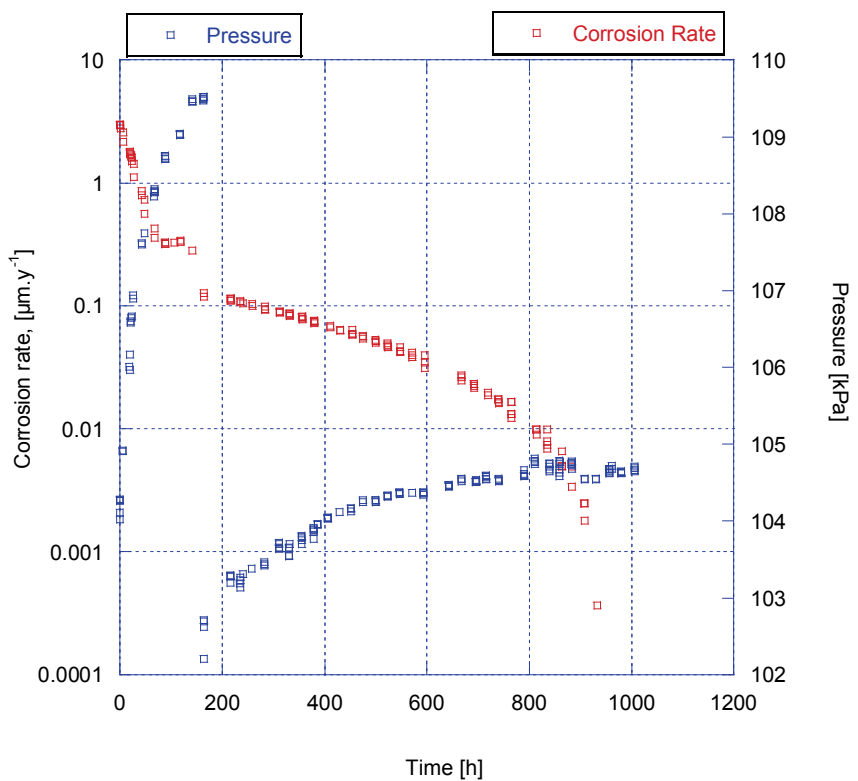


Figure 27: Corrosion behaviour of pickled wires exposed to 70°C, 100% RH

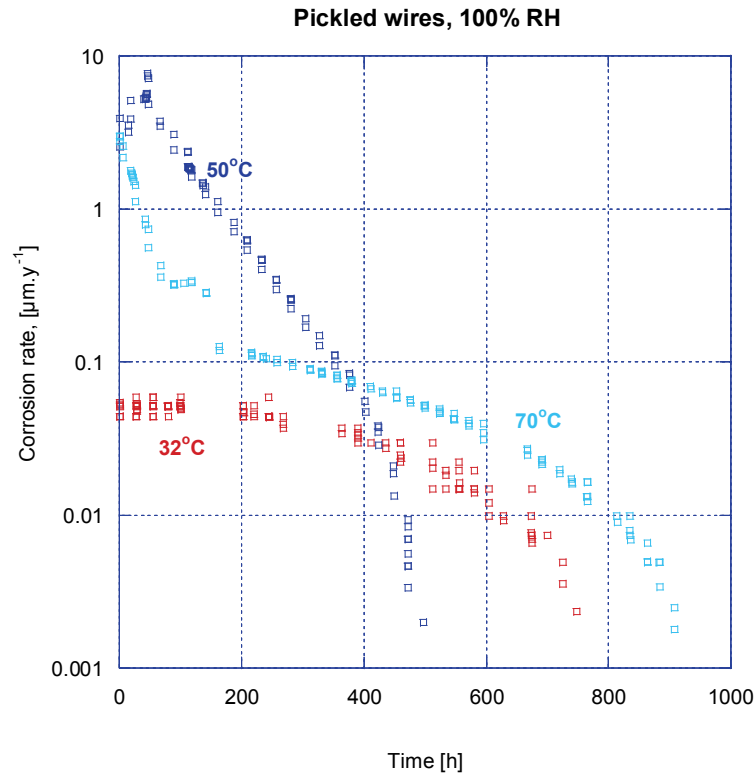


Figure 28: Corrosion behaviour of pickled wires exposed to 100% RH

Testing with degreased wires showed less corrosion, as expected. These wires have a well-formed air oxide prior to exposure.

Some attempts were made to fit decay functions to the corrosion transients obtained in these tests. For the pickled wires at 32°C and 100% RH (data of Figure 25), the corrosion rate appeared to decay linearly to zero – not a normal functional form for a corrosion-rate decay, but perhaps informative – Figure 27. At 50°C, the decay took on a definite exponential form with a time constant of about 100 hours – Figure 30. At 70°C, the fit was less impressive but as the eye would indicate, the time constant was shorter – close to 10 hours - Figure 31.

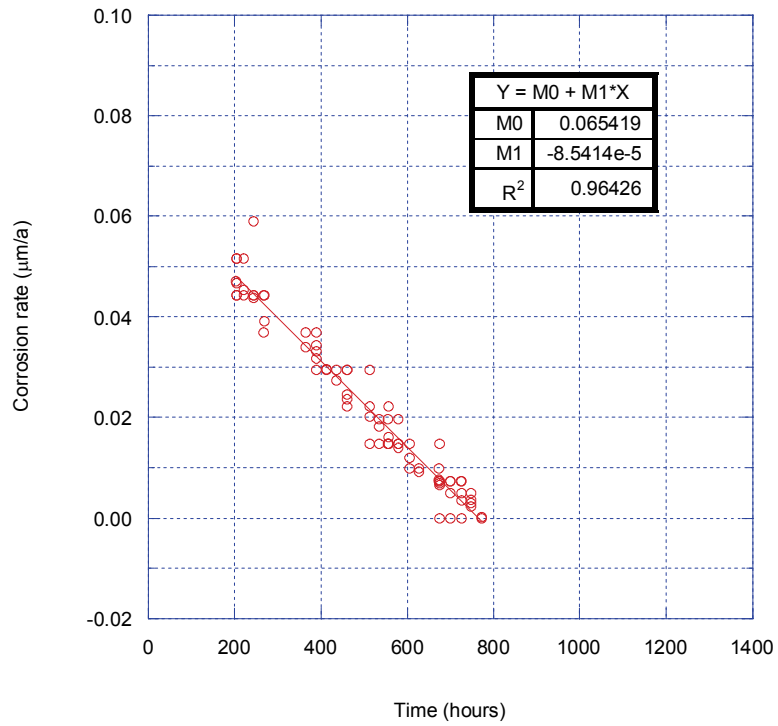


Figure 29: Linear curve fit of corrosion rates, pickled wires exposed to 32°C and 100% RH

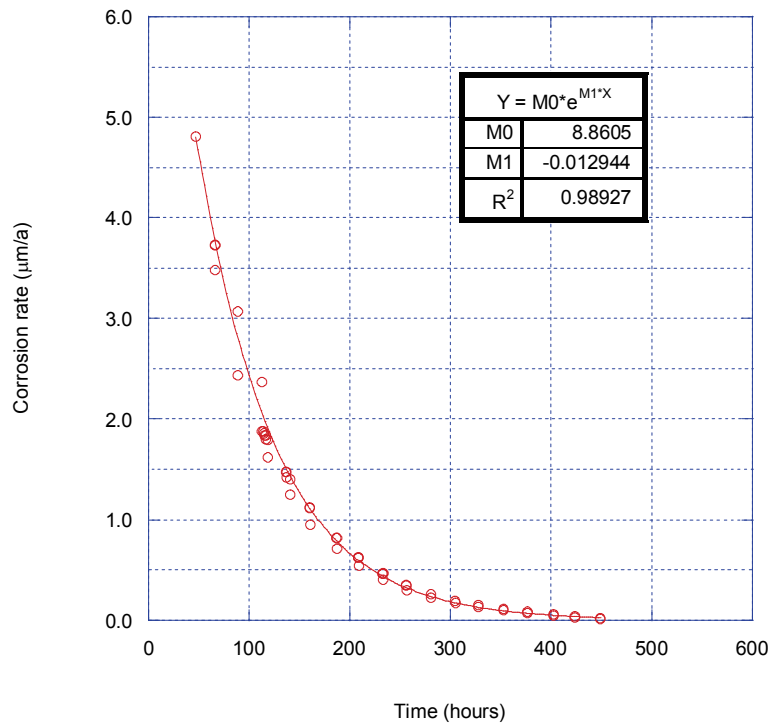


Figure 30: Exponential curve fit of corrosion rates, pickled wires exposed to 50°C and 100% RH

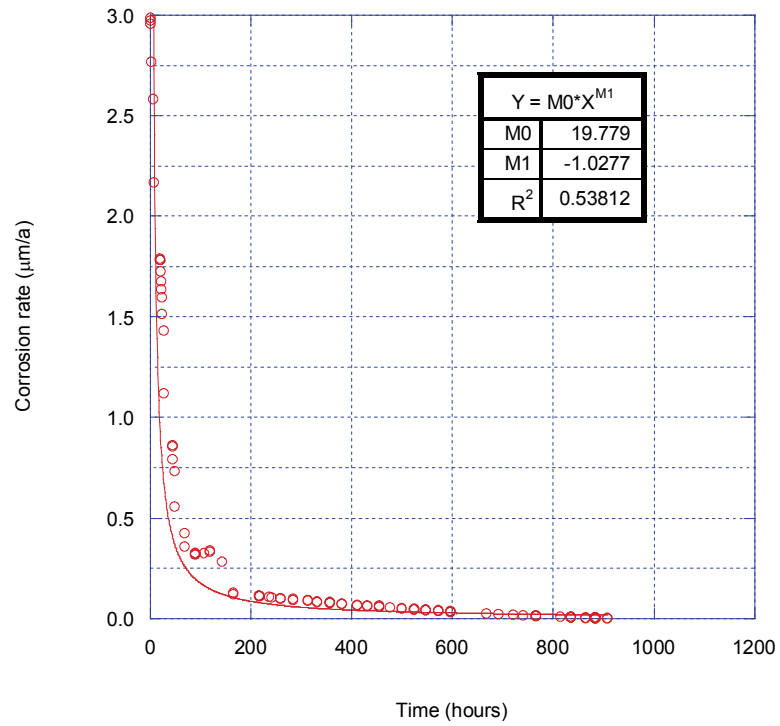


Figure 31: Power curve fit of corrosion rates, pickled wires, exposed to 70°C and 100% RH

The faster corrosion-rate decay at 70°C than at 50°C is perhaps to be expected, as magnetite can more easily form at higher temperatures and is expected to be more protective than Fe(OH)₂.

3.2 Copper Cell – H₂ Sensor Experiments

Table 7 shows the meaningful results obtained with the hydrogen sensor, selected from a large number of tests most of which were flawed in one way or another. Where a corrosion rate is mentioned, it is the average over the mentioned interval; then the cell is flushed with nitrogen and the p_{H2} is reset to zero (but the metal samples are not replaced).

Table 7: H₂ sensor experimental results

Test Condition	Interval between Measurement time increment	Estimated Corrosion Rate (average over increment)
Pickled wires, 85% RH, 50°C		
1 st measurement	164 hrs	1.1 x 10 ⁻⁴ μm·y ⁻¹
2 nd measurement	259 hrs	1.0 x 10 ⁻⁴ μm·y ⁻¹
3 rd measurement	313 hrs	1.6 x 10 ⁻⁴ μm·y ⁻¹
4 th measurement	235 hrs	2.5 x 10 ⁻⁴ μm·y ⁻¹
5 th measurement	262 hrs	2.0 x 10 ⁻⁴ μm·y ⁻¹
6 th measurement	332 hrs	2.4 x 10 ⁻⁴ μm·y ⁻¹
7 th measurement	221 hrs	3.1 x 10 ⁻⁴ μm·y ⁻¹
Pickled wires, 75% RH, 50°C		
1 st measurement	353 hrs	7.0 x 10 ⁻⁵ μm·y ⁻¹
2 nd measurement	359 hrs	1.8 x 10 ⁻⁴ μm·y ⁻¹
3 rd measurement	310 hrs	3.1 x 10 ⁻⁴ μm·y ⁻¹
4 th measurement	216 hrs	4.8 x 10 ⁻⁴ μm·y ⁻¹
5 th measurement	283 hrs	---
6 th measurement	260 hrs	---
7 th measurement	408 hrs	3.3 x 10 ⁻⁴ μm·y ⁻¹
8 th measurement	212 hrs	6.3 x 10 ⁻⁴ μm·y ⁻¹
9 th measurement	218 hrs	4.9 x 10 ⁻⁴ μm·y ⁻¹
10 th measurement	91 hrs	1.01 x 10 ⁻³ μm·y ⁻¹
Pickled wires, 100% RH, 50°C		
1 st measurement	473 hrs	---
2 nd measurement	93 hrs	6.7 x 10 ⁻³ μm·y ⁻¹
3 rd measurement	93 hrs	2.5 x 10 ⁻³ μm·y ⁻¹

These tests are important, but preliminary. The meaning of the apparent increase in corrosion rate with time is not clear. We cannot tell, at this stage, whether this is a real phenomenon, or an artefact of the extremely low amount of incremental oxidation that occurs in each batch stage of the reaction, combined with the perturbation of removing the hydrogen formed during the previous stage. Nevertheless, this is a historically important result, in that it is certainly the lowest corrosion rate that has ever been measured in such an environment. Regarding the repository, such rates would appear not to pose much of a threat.

3.3 Surface Analyses

Detailed surface analysis results and survey spectra data are presented in a separate report prepared by Surface Science Western of the University of Western Ontario (SSW 2010). Interesting findings from the various surface analyses and result summaries are discussed in the following sections.

Table 8 lists the samples selected for surface analysis and microscopy. Note that '0.5M NaCl coated' denotes samples that were pre-immersed in the stated solution for 10 minutes, then dried in an oven set at 50°C overnight to leave a salt deposit; 'precorroded' is an alternative term used elsewhere in this report.

Table 8: 15 samples examined by surface analyses

Sample #	Condition	RH	Temp	Duration
1	Control, no previous exposure, wires degreased in acetone	--	--	--
2	Control, no previous exposure, wires coated with 0.5M NaCl (no rinse before analyses)	--	--	--
3	Degreased wires (w/ acetone), exposed to deaerated environment (using N ₂)	100%	50°C	615 hrs
4	Pickled wires (w/ HCl)	100%	50°C	1001 hrs
5	Pickled wires (II)	100%	50°C	688 hrs
6	0.5M NaCl dipped wires, no rinse before analyses	75%	50°C	370 hrs
7	0.5M NaCl dipped wires, rinsed before analyses	75%	50°C	370 hrs
8	Degreased wires, exposed to anoxic environment (deaerated w/ N ₂ / H ₂)	100%	50°C	591 hrs
9	0.5M NaCl dipped wires, no rinse before analyses	100%	50°C	237 hrs
10	0.5M NaCl dipped wires, rinsed before analyses	100%	50°C	237 hrs
11	Pickled wires	100%	70°C	1006 hrs
12	Pickled wires	74.1%	70°C	1121 hrs
13	Raw steel wires for XPS sputtering experiment	--	400°C	Heated in air, 3 hrs
14	0.5M NaCl dipped wires, no rinse before analyses	100%	50°C	1725 hrs
15	0.5M NaCl dipped wires, rinsed before analyses	100%	50°C	1725 hrs

3.3.1 XPS

Table 9 lists the apparent near-surface atomic compositions obtained from XPS survey spectra of all the samples, without any sputter etching except for sample 13. This sample was used to determine the elemental ratios that would exist on a well-characterized, oxidized iron surface after sputter etching – evidently a good 2:3 Fe:O ratio is found after 1 minute sputtering, but after 5 minutes there is evidence of film reduction.

Table 9: Composition data from XPS survey scan spectra

Sample		Composition (at. %)									
		Fe	C	O	Na	Cl	F	Mn	Si	N	Ca
1	Area 1	13	42.4	40.6	0.3	0.5		0.5	1.2	0.7	0.8
2	Area 1	22.4	19.8	49.1	3.0	4.5		0.9		0.3	0.1
3	Area 1	4.3	48.6	39.9		0.5		0.9	3.9	0.9	1.2
4	Area 1	10.8	39.3	44.7		0.2			3.9	1.1	
5	Area 1	12.2	42.1	43.2		0.7			1.7		
6	Area 1	20.5	27.0	49.5	0.8	0.9			1.2		
7	Area 1	18.1	27.6	51.8	1.1	0.8			0.7		
8	Area 1	3.4	49.4	40.3					6.1		0.8
9	Area 1	13.7	34.0	47.5	3.0	1.9					
10	Area 1	18.1	28.8	51.1		0.5				1.5	
11	Area 1	12.5	40.7	44.6			2.2				
12	Area 1	13.2	40.0	41.3		0.6			3.7	1.2	
13	As-heated	14.0	42.2	43.3	0.6						
	After 1 min sputtering	36.3	11.5	51.8	0.4						
	After 5 min sputtering	31.9	7.9	59.9	0.4						
14	Area 1	20.4	29.3	42.8	0.3	4.2					
15	Area 1	15.0	40.8	43.9		0.4					

Table 10 lists the results of fitting of high-resolution XPS spectra. This information is not all useful, but indicates the following broad findings –

- A Fe metal peak is found in a number of spectra, indicative of a thin oxide film, a few nm at most, with lower apparent Fe metal content corresponding to thicker films.
- Fe III species are found in many surfaces, which indicate (for samples previously exposed to anoxic conditions) that the precautions taken to avoid air exposure were not wholly successful
- FeO is sometimes found according to the peak fitting; this assignment should be taken with a pinch of salt.
- Carbonate species are again indicative of an interaction with the atmosphere after anoxic exposure.

Table 10: Summary of XPS high-resolution spectra data

Sample	XPS Summary
1	Fe metal 4.3%, Fe ₂ O ₃ : 70.4%; FeO: 25.3%; film thickness: ~ 6 nm
2	Fe ₂ O ₃ : 60.6%; Fe ₃ O ₄ : 2.3%; FeOOH: 37.1%
3	Fe metal: 6.1%; Fe ₂ O ₃ : 47.9%; Fe ₃ O ₄ : 19.5%; FeOOH: 26.4%; film thickness: ~ 5.7 nm
4	Fe metal: 2.1%; Fe ₂ O ₃ : 30.6%; Fe ₃ O ₄ : 48.6%; FeOOH: 18.7%; film thickness: ~ 7.5 nm
5	Fe metal: 1.8%; Fe ₂ O ₃ : 29.6%; Fe ₃ O ₄ : 41.8%; FeOOH: 26.9%; film thickness: ~ 7.8 nm
6	FeCO ₃ : 63.9%; Fe ₂ O ₃ : 11.2%; FeO: 24.7%
7	FeCO ₃ : 64.6%; Fe ₂ O ₃ : 15.7%; FeO: 19.7%
8	Fe metal: 4.8%; Fe ₃ O ₄ : 26.2%; FeOOH: 10.3%; Fe ₂ O ₃ : 58.9%
9	FeCO ₃ : 60.1%; Fe ₂ O ₃ : 3.9%; FeO: 35.9%
10	Fe metal: 1.9%; Fe ₃ O ₄ : 50.4%; FeOOH: 5.2%; Fe ₂ O ₃ : 42.6%
11	Fe ₃ O ₄ : 60.9%; Fe ₂ O ₃ : 39.1%
12	Fe ₃ O ₄ : 49.3%; FeOOH: 29.4%; Fe ₂ O ₃ : 21.5%
13	Steel wire oxidized in air at 400°C and found to contain a mixture of Fe ₂ O ₃ /Fe ₃ O ₄ in XPS analysis. Upon sputtering, the well-defined oxide (mixture) is reduced and is sufficiently damaged to make curve-fitting of the resulting spectra difficult. Peak widths are broadened significantly and metallic iron is formed.
14	Appears to be a mixture of Fe ₂ O ₃ , Fe ₃ O ₄ and FeCO ₃ . FeOOH may also be present.
15	Appears to be a mixture of Fe ₂ O ₃ , Fe ₃ O ₄ and FeCO ₃ . FeCO ₃ levels are much lower than sample 14. FeOOH may also be present.

3.3.2 SEM/EDX

Table 11 gives the results of EDX analysis, with some indication of the spatial variability of average composition within the analysis depth, which is much greater than that of XPS. Oxygen levels give a broad indication of which films have substantial thickness, of the order of at least 0.1 micron. These correspond, as expected, to the more aggressive conditions.

Table 11: Composition data from EDX analyses

Sample		Composition (at. %)									
		Fe	C	O	Na	Cl	S	Mn	Ca	Al	Si
1	Area 1	100									
	Area 2	100									
2	Area 1	60.7		27.7	8.5	3.2					
	Area 2	62.3		30.7		6.9					
	Area 3	71.3		11.7	11.0	6.1					
	Area 4	71.8		19.7		8.5					
3	Area 1	71.4	28.1					0.3			0.2
	Area 2	86.7	12.8					0.3			0.2
4	Area 1	83.1	9.7	6.9							0.2
	Area 2	60.3	33.6	6.1							
5	Area 1	55.7	25.3	18.9			0.1				
	Area 2	81.8	11.6	6.1				0.3			0.2
6	Area 1	46.5	19.4	33.1	0.4	0.3		0.3			
	Area 2	64.6		32.3	0.9	0.3		0.3		1.5	0.2
7	Area 1	64.0		33.5	1.1	0.4	0.4		0.5		0.2
	Area 2	49.5	14.4	35.1	0.4	0.4					0.1
8	Area 1	89.5	8.26	1.24			0.55	0.42			
	Area 2	88.0	9.52	1.66			0.38	0.4			
9	Area 1	64.9		30.7	2.19	1.96		0.29			
	Area 2	64.9		31.1	2.24	1.76					
10	Area 1	60.2	12.0	27.8							
	Area 2	80.1		19.5		0.08		0.32			
11	Area 1	86.2	10.1	3.70							
	Area 2	81.7	14.0	4.30							
12	Area 1	82.3	13.9	3.40				0.3	0.1		
	Area 2	72.0	22.9	5.00					0.1		
14	Area 1	62.2	14.4	22.1	0.8	0.1		0.3	0.1	0.1	
	Area 2	61.2	15.2	22.4	0.8	0.1		0.3	0.1		
15	Area 1	58.7	20.2	20.9				0.3			
	Area 2	57.5	17.8	24.3				0.2	0.1		

3.3.3 Raman Spectroscopy and Fourier Transform Infrared (FTIR) Spectroscopy

Table 12 lists the findings of Raman spectroscopy analysis. It should be noted that this technique is not sensitive to $\text{Fe}(\text{OH})_2$ (Odziemkowski et al. 1998). However, to the extent that Fe_3O_4 is positively identified, this clarifies the nature of the films formed in anoxic conditions. The formation of some Fe III oxide or oxyhydroxide, or carbonates, by exposure to traces of oxygen does not invalidate this basic finding. Yet we cannot say, at this point, what are the relative amounts of Fe_3O_4 and $\text{Fe}(\text{OH})_2$ in these products, and diffraction would not necessarily help, as many of the films are thin and $\text{Fe}(\text{OH})_2$ is always poorly crystalline. Some evidence towards a preponderance of Fe_3O_4 is the lack of positive evidence for OH in the FTIR data, but these spectra were weak.

Table 12: Summary of Raman and FTIR spectra data

Sample	Spectra data
1	Fe_3O_4 , could be FeO and amorphous carbon
2	Fe_3O_4 , α - FeOOH , likely carbonate species, amorphous carbon and other iron species such as maghemite (γ - Fe_2O_3) and ferrihydrite (generally presented as $\text{Fe}_2\text{HO}_8 \cdot 4\text{H}_2\text{O}$, also written as $5 \text{Fe}_2\text{O}_3 \cdot 9\text{H}_2\text{O}$ or as $\text{Fe}_2\text{O}_3 \cdot 2\text{FeOOH} \cdot 2.6\text{H}_2\text{O}$)
3	Raman analysis did not find any evidence of oxide species on this sample.
4	Typical of Fe_3O_4 .
5	Typical of Fe_3O_4 . No other oxide species were detected.
6	Amorphous carbon, Fe_3O_4 , Fe_2O_3 and gamma and alpha Fe_2O_3 .
7	Fe_3O_4 , carbonate, beta- $\text{FeOOH}(\text{Cl})$, and gamma- Fe_2O_3 .
8	<u>Raman</u> : Amorphous carbon and Fe_3O_4 . <u>FTIR</u> : Weak with no assignable peaks
9	<u>Raman</u> : Fe_3O_4 , carbonate and amorphous carbon. <u>FTIR</u> : Likely mixed carbonate/hydroxide species.
10	<u>Raman</u> : Fe_3O_4 , amorphous carbon, alpha FeOOH , Fe_2O_3 , gamma- Fe_2O_3 and carbonate. <u>FTIR</u> : Likely mixed carbonate/hydroxide species.
11	<u>Raman</u> : spectra are consistent with Fe_3O_4 with some contribution from amorphous carbon. <u>FTIR</u> : spectra are very weak and undifferentiated. No evidence of hydroxide.
12	<u>Raman</u> : spectra are consistent with Fe_3O_4 with some contribution from amorphous carbon. <u>FTIR</u> : No evidence of hydroxide in the FTIR spectra.
13	Sample not examined using Raman
14	<u>Raman</u> : presence of mainly Fe_3O_4 with some areas showing the presence of gamma- Fe_2O_3 (maghemite). <u>FTIR</u> : mainly showed the presence of broad undifferentiated peaks which were not assigned.
15	<u>Raman</u> : presence of Fe_3O_4 , with some areas also showing the presence of a peak likely arising from carbonates. <u>FTIR</u> : spectra were weak in some areas and strong in others. The strong spectra were consistent with the spectra observed previously and proposed as arising from a mixed carbonate/hydroxide species.

4. DISCUSSION OF SURFACE ANALYSIS RESULTS

Figure 32 shows the mixture of salt deposit and corrosion product that was the starting point for the NaCl 'coated' or 'precorroded' tests (images of Sample 2). Heavy deposits are found on wires surfaces.

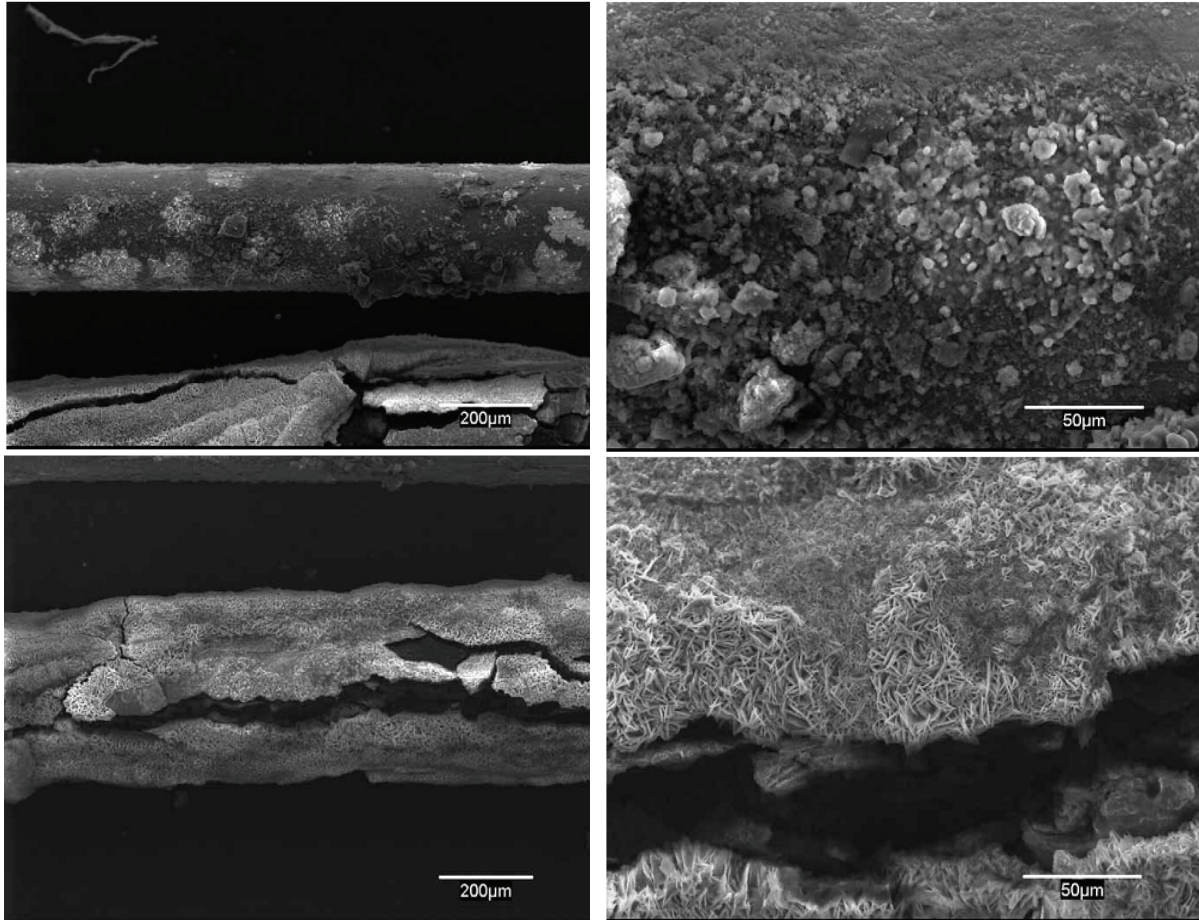


Figure 32: SEM images of Sample 2 (3rd and 4th wires) - 0.5M NaCl coated wires

Figure 33 shows roughly circular patches that were found on some samples exposed to 100% RH without salt coating; these are possibly centred on manganese sulfide inclusions, but the necessary analyses (e.g. by spatially resolved XPS or Auger Electron Spectroscopy) were not carried out.

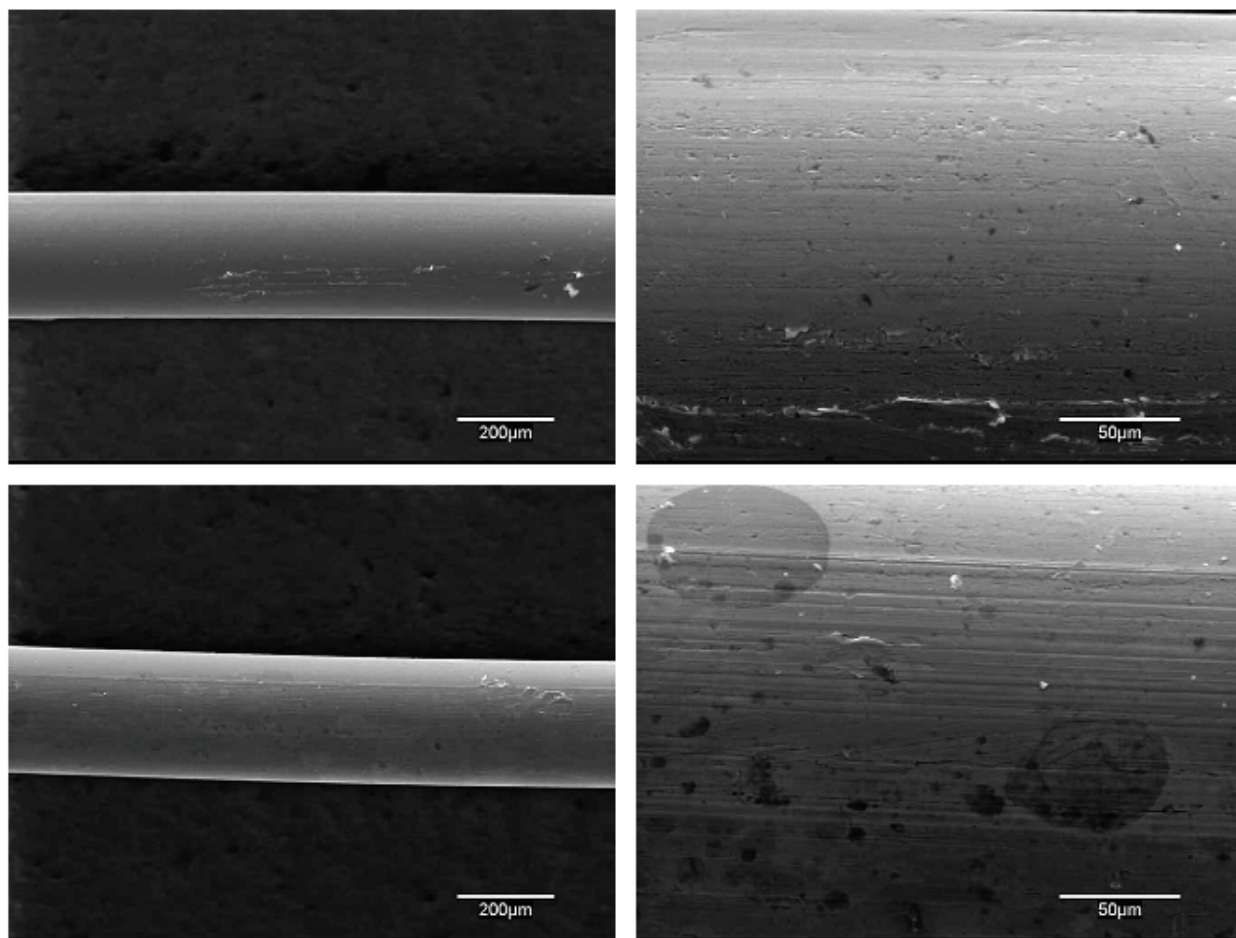
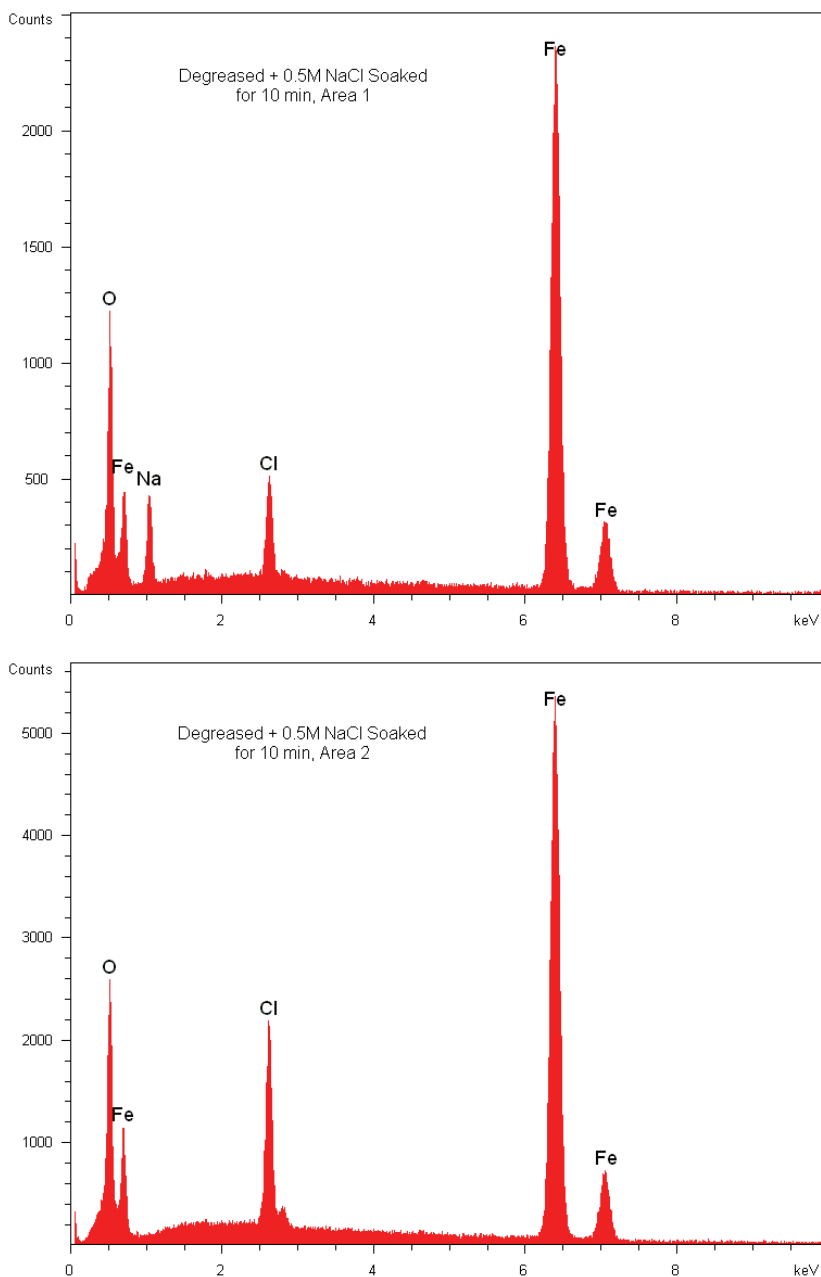
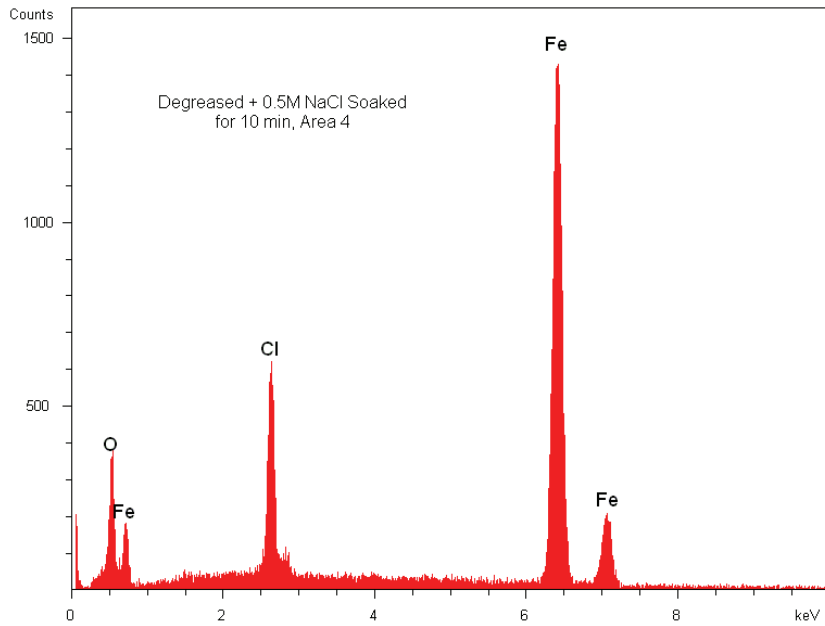
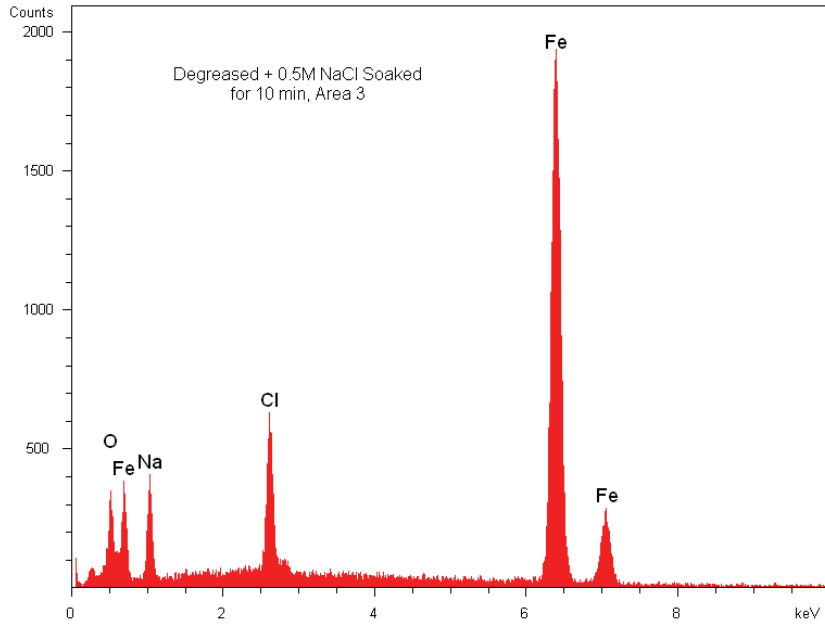


Figure 33: SEM images of Sample 3 - degreased wires, 50°C, 100% RH

Figure 34 shows that regions can be isolated in the salt-coated surface that contain salt crystals or are composed purely of corrosion product. It should be noted that the use of ordinary air and water exposure for this NaCl pretreatment could account for the presence of Fe III species or carbonates in the corrosion products after anoxic exposure, but examination of the full range of data reveals that there must have been some post-air exposure as well. Regarding the Fe III species, it would be expected that hydrogen from anoxic corrosion would reduce these to magnetite or Fe II species, but such reactions may be slow.

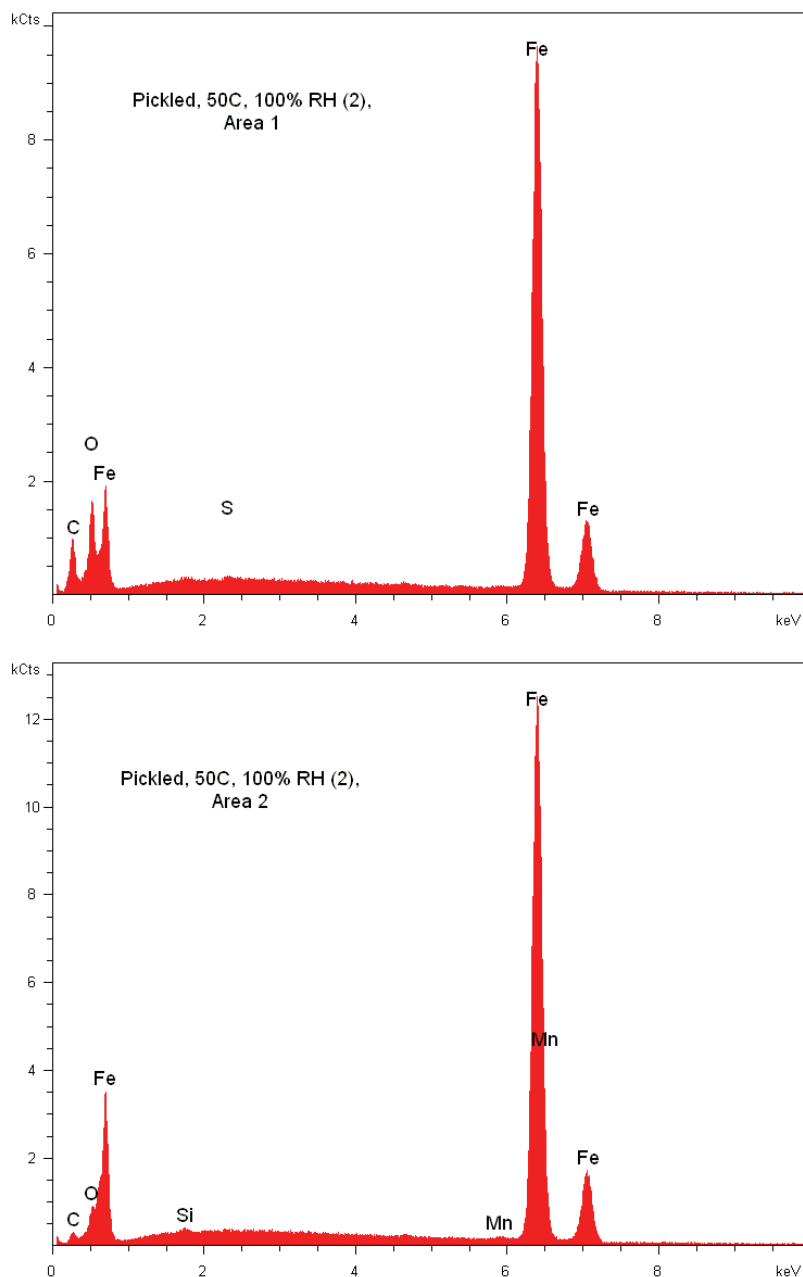




EDX results in weight percent				
Analysis	O	Na	Cl	Fe
Analysis 1	27.7	8.5	3.2	60.7
Analysis 2	30.7		6.9	62.4
Analysis 3	11.7	11.0	6.1	71.3
Analysis 4	19.7		8.5	71.8

Figure 34: EDX spectra of Sample 2 - control, 0.5M NaCl coated wires

Generally EDX did not give much information on samples that were exposed to anoxic conditions without a salt deposit, but oxygen was detectable in some cases, as shown in Figure 35.

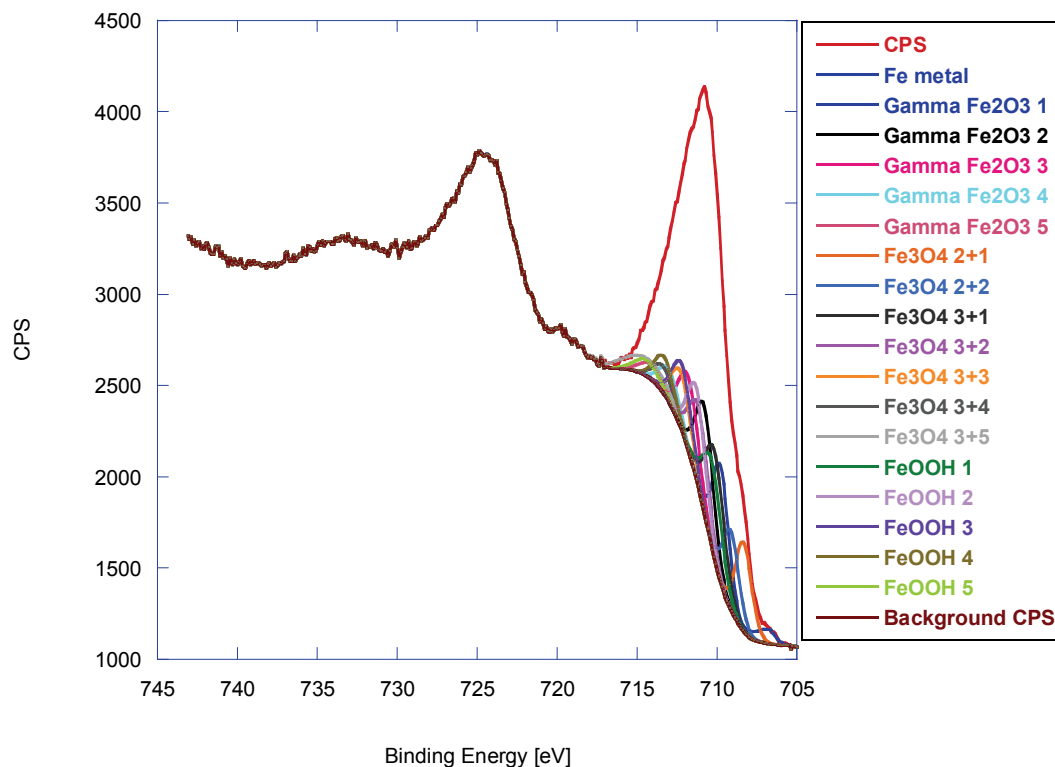


EDX results in weight percent						
Analysis	C	O	Si	S	Mn	Fe
Analysis 1	25.3	18.9		0.1		55.7
Analysis 2	11.6	6.1	0.2		0.3	81.8

Figure 35: EDX spectra of Sample 5 - pickled wires (II), 50°C and 100% RH

Figure 36 is included as an example of a high-resolution XPS spectrum for one of the thinner films formed under anoxic conditions. The take-off angle was large (90 degrees), so the analysis depth is maximized. The number of species to which the iron spectrum is fitted is at the limit of our ability to deconvolute such spectra; however the presence and approximate quantity of the different formal oxidation states (0, 2.66 and 3) should be fairly reliable (i.e. 1-2% Fe metal, 42% Fe₃O₄, 30% Fe₂O₃, and 27% FeOOH). The Fe III species indicate some effect of air exposure despite the precautions taken. The presence of a signal from Fe metal shows that the oxide layer is thin. The analysts do not claim to find Fe II species such as Fe(OH)₂. The estimated film thickness is given as 7.8 nm, but this cannot be expected to be very accurate in view of the small contribution of Fe metal to the spectrum. Based on the integrated hydrogen production in the anoxic exposure (Figure 26), 27 nm of Fe₃O₄ was estimated to be formed according to the pressure measurements (this calculation is presented in Appendix E). Possible explanations for the discrepancy in the two thicknesses are that the mass of the film is dominated by locally thicker areas, or (most likely) that the metallic Fe signal is only roughly estimated.

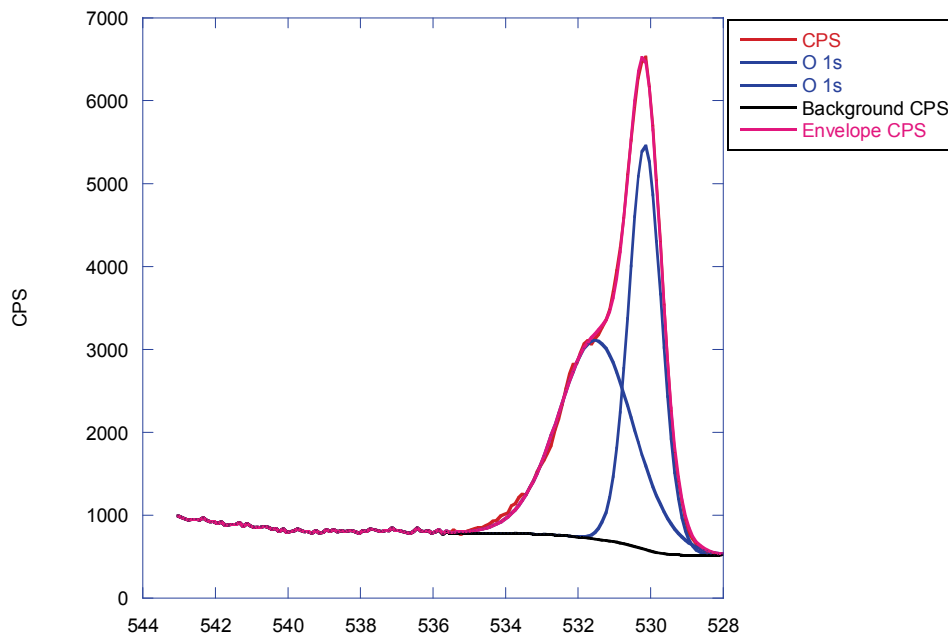
Sample 5 - Pickled wires, 50°C, 100%RH, Fe(2p) high resolution spectrum



Name	Pos.	FWHM	L.Sh.	Area	% Area
Fe metal	706.79	0.95	LA(1.2,4.8,3)	161.6	1.8
Gamma Fe ₂ O ₃ 1	709.78	1.20	GL(30)	828.7	9.1
Gamma Fe ₂ O ₃ 2	710.78	1.30	GL(30)	828.7	9.1
Gamma Fe ₂ O ₃ 3	711.78	1.40	GL(30)	613.9	6.7
Gamma Fe ₂ O ₃ 4	712.98	1.40	GL(30)	275.2	3.0
Gamma Fe ₂ O ₃ 5	714.08	1.70	GL(30)	154.2	1.7
Fe ₃ O ₄ 2+1	708.35	1.20	GL(30)	631.6	6.9
Fe ₃ O ₄ 2+2	709.15	1.20	GL(30)	563.1	6.2
Fe ₃ O ₄ 3+1	710.15	1.40	GL(30)	901.7	9.9
Fe ₃ O ₄ 3+2	711.15	1.40	GL(30)	677.2	7.4
Fe ₃ O ₄ 3+3	712.25	1.40	GL(30)	464.2	5.1
Fe ₃ O ₄ 3+4	713.35	1.40	GL(30)	216.9	2.4
Fe ₃ O ₄ 3+5	714.45	3.30	GL(30)	346.2	3.8
FeOOH 1	710.30	1.40	GL(30)	720.2	7.9
FeOOH 2	711.30	1.30	GL(30)	706.8	7.8
FeOOH 3	712.20	1.40	GL(30)	549.5	6.0
FeOOH 4	713.3	1.40	GL(30)	308.6	3.4
FeOOH 5	714.40	1.80	GL(30)	168.0	1.8

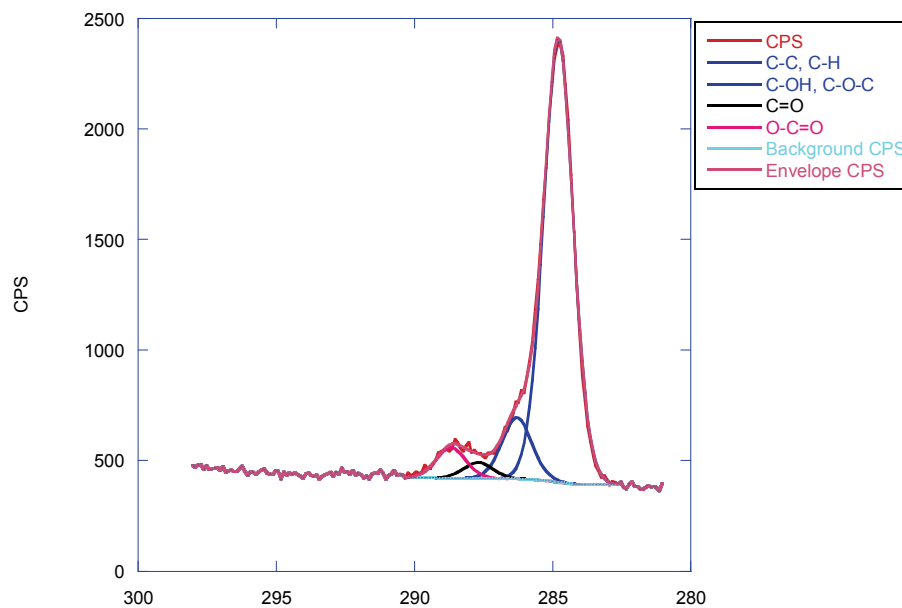
Fe metal 1.8%
 Fe₂O₃ 29.6%
 Fe₃O₄ 41.8%
 FeOOH 26.9%
 Film thickness ~ 7.8 nm

Sample 5 - Pickled wires, 50°C, 100%RH, O 1s high resolution spectrum



Name	Pos.	FWHM	L.Sh.	Area	% Area
O 1s	531.51	2.45	GL(30)	6365.8	53.3
O 1s	530.16	1.06	GL(30)	5572.8	46.7

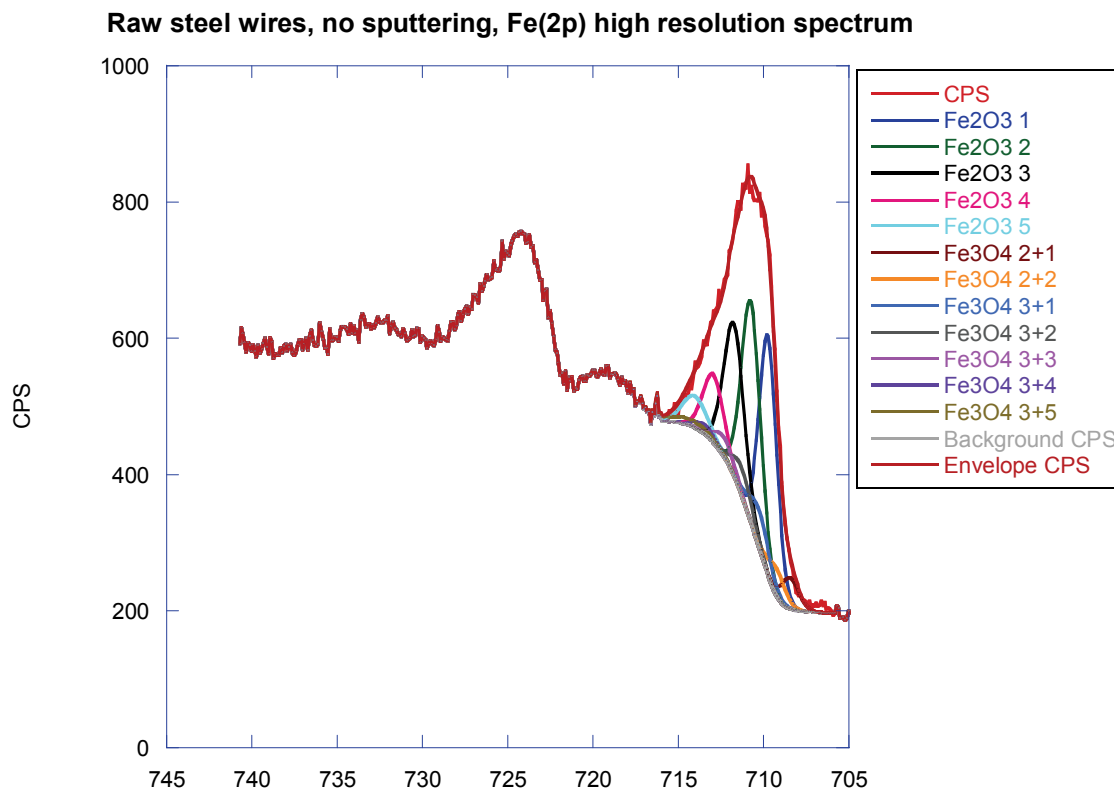
Sample 5 - Pickled wires, 50°C, 100%RH, C 1s high resolution spectrum



Name	Pos.	FWHM	L.Sh.	Area	% Area
C-C, C-H	284.80	1.25	GL(30)	2711.4	80.3
C-OH, C-O-C	286.30	1.25	GL(30)	377.3	11.2
C=O	287.70	1.25	GL(30)	97.9	2.9
O-C=O	288.69	1.25	GL(30)	188.7	5.6

Figure 36: XPS high resolution spectra of Sample 5 - pickled wires (II), 50°C, 100% RH

High-resolution XPS spectra of the iron wire heated at 400°C, before and after sputter etching, are shown in Figure 37. No metallic Fe is found on the outer surface, but partial film reduction occurs during sputtering. These spectra are however useful for interpretation of the spectra of the corroded surfaces.



Name	Pos.	FWHM	L.Sh.	Area	% Area
Fe ₂ O ₃ 1	709.75	1.20	GL(30)	457.3	24.8
Fe ₂ O ₃ 2	710.75	1.30	GL(30)	457.3	24.8
Fe ₂ O ₃ 3	711.75	1.40	GL(30)	338.8	18.4
Fe ₂ O ₃ 4	712.95	1.40	GL(30)	151.9	8.2
Fe ₂ O ₃ 5	714.05	1.70	GL(30)	85.1	4.6
Fe ₃ O ₄ 2+1	708.45	1.20	GL(30)	58.8	3.2
Fe ₃ O ₄ 2+2	709.25	1.20	GL(30)	52.4	2.8
Fe ₃ O ₄ 3+1	710.25	1.40	GL(30)	84.0	4.6
Fe ₃ O ₄ 3+2	711.25	1.40	GL(30)	63.1	3.4
Fe ₃ O ₄ 3+3	712.35	1.40	GL(30)	43.2	2.3
Fe ₃ O ₄ 3+4	713.45	1.40	GL(30)	20.2	1.1
Fe ₃ O ₄ 3+5	714.55	3.30	GL(30)	32.2	1.7

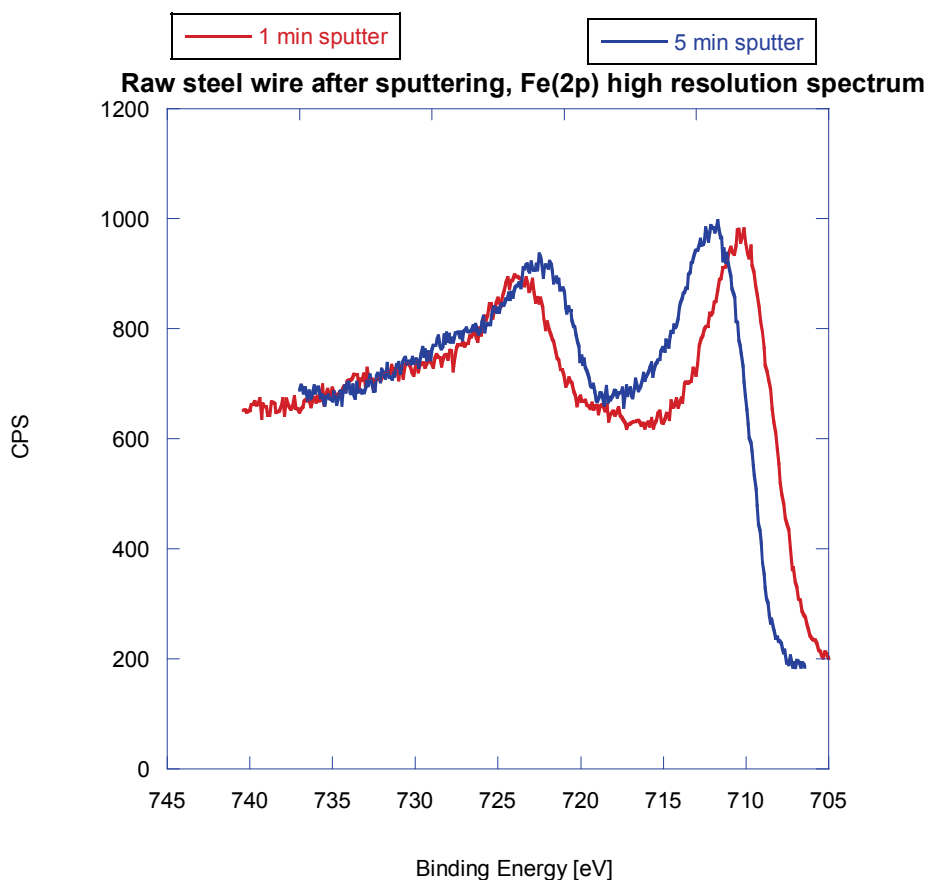


Figure 37: XPS analysis of raw steel wires

Figure 38a shows an example of a Raman spectrum for an anoxic test without salt coating that gave a relatively thin oxide film, showing a well-resolved feature ascribed to Fe_3O_4 . A total of 5 areas on different wires were analyzed. All spectra consistently show a peak near 667 cm^{-1} , typical of Fe_3O_4 . The broad undifferentiated feature around 450 cm^{-1} comes from the NMR tube in which the sample was encapsulated. Another area of the same sample showed a more intense peak typical of Fe_3O_4 – Figure 38b. More representative spectra were obtained by subtracting the spectrum of the NMR tube – Figure 38c.

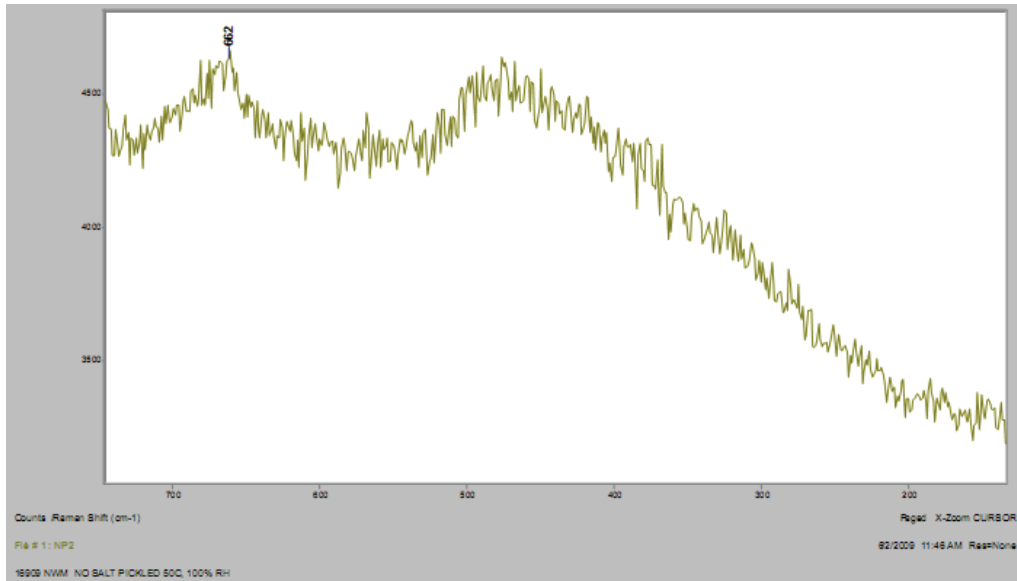


Figure 38 a: Raman spectrum of Sample 4 - pickled wires, 50°C, 100% RH

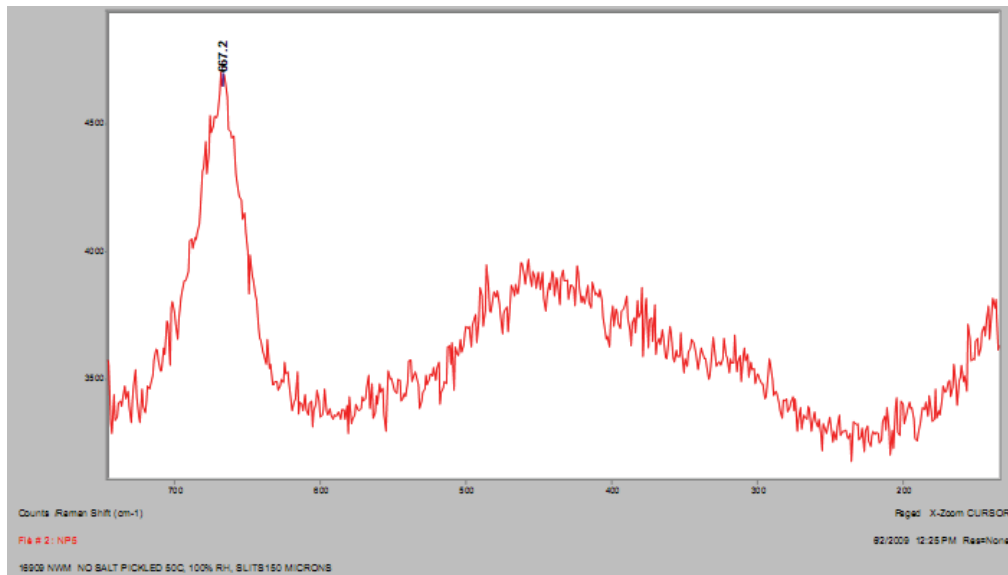


Figure 38 b: Raman spectrum of Sample 4 - pickled wires, 50°C, 100% RH

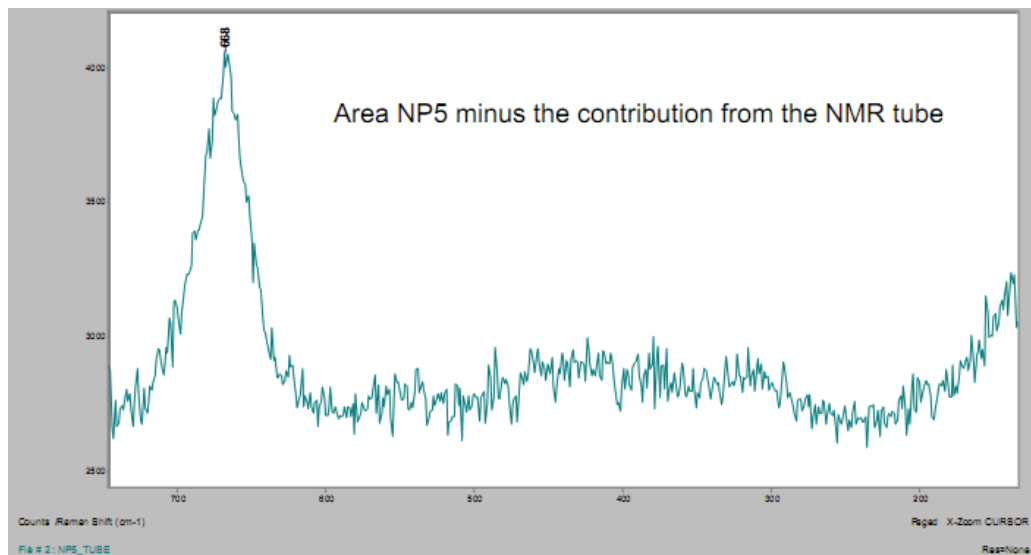


Figure 38 c: Raman spectrum of Sample 4 - pickled wires, 50°C, 100% RH

Figure 39a shows the SEM images of Sample 7 – 0.5M NaCl coated wires, exposed to 75% RH and 50°C for ~ 370 hours. Samples rinsed after anoxic testing with a salt coating showed significant development of corrosion products compared with their condition before exposure, consistent with the amount of metal oxidized as deduced from hydrogen pressure increase. Large oxygen peaks are shown in EDX spectra, Figure 39b.

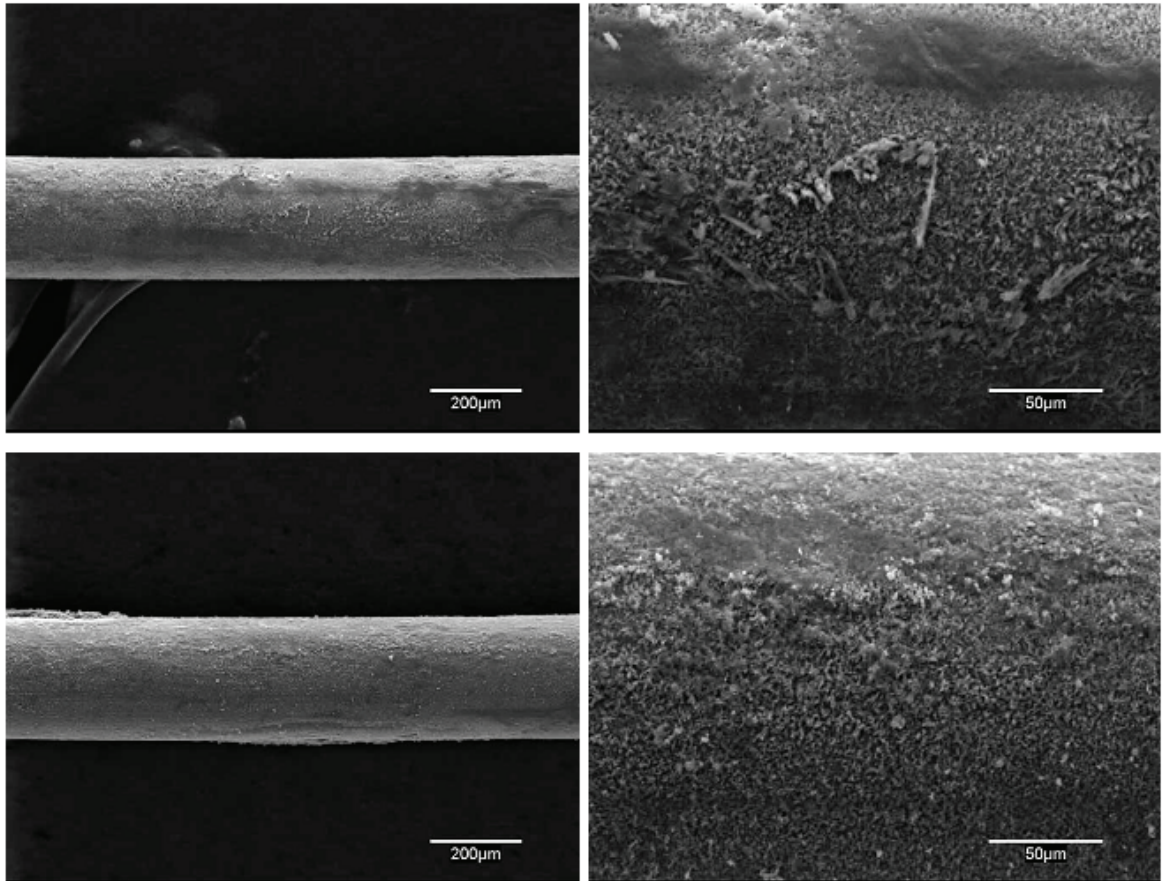
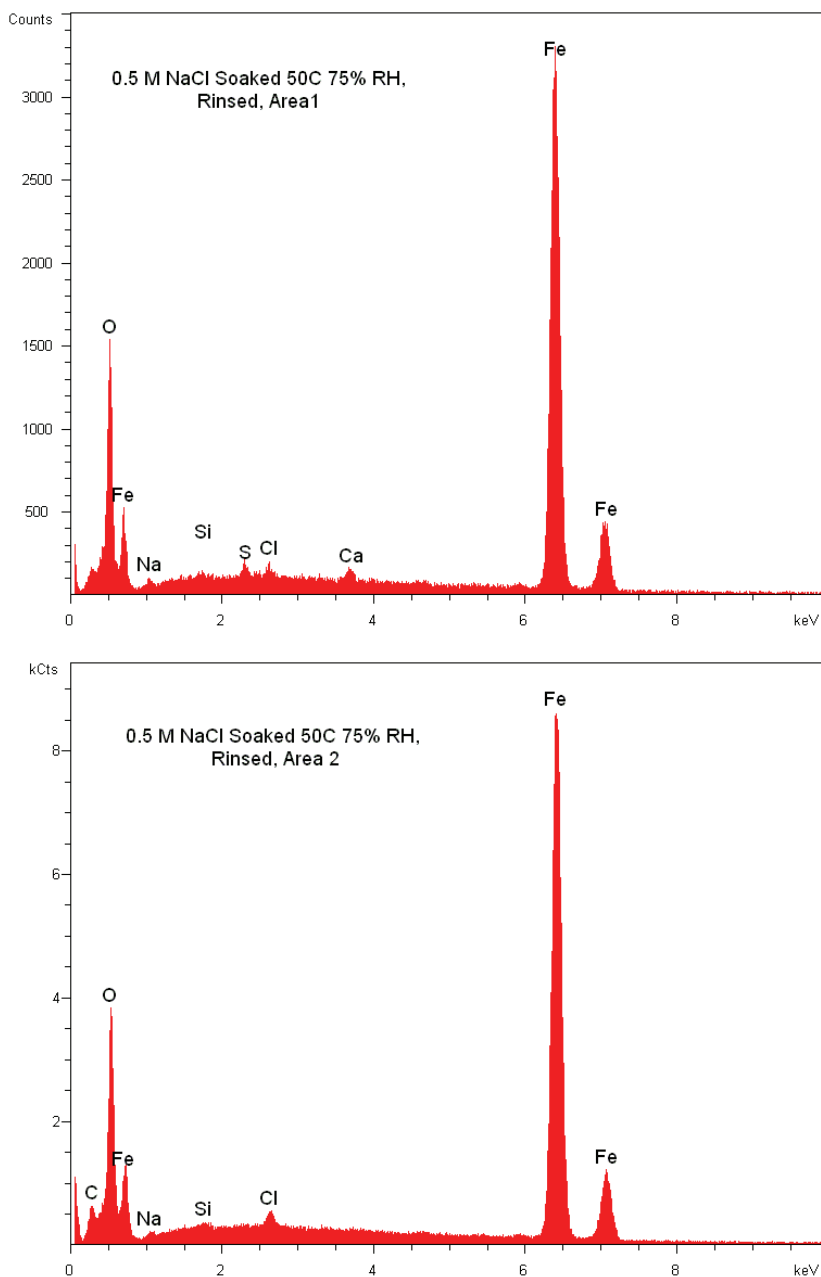


Figure 39 a: SEM images of Sample 7 - 0.5M NaCl coated wires, 50°C, 75% RH



EDX results in weight percent								
Analysis	C	O	Na	Si	S	Cl	Ca	Fe
Analysis 1		33.5	1.1	0.2	0.4	0.4	0.5	64.0
Analysis 2	14.4	35.1	0.4	0.1		0.4		49.5

Figure 39 b: EDX spectra of Sample 7 - 0.5M NaCl coated wires, 50°C, 75% RH

Raman spectra from samples tested in anoxic conditions with salt coating showed intense peaks indicative of various iron oxides or oxyhydroxides – Figures 40a & 40b. Some areas showed mostly Fe_3O_4 , while others showed complex mixtures, leading to the speculation that some products fell off the surface during rinsing, although this was done as gently as possible. We believe that the new corrosion product formed during anoxic exposure was nearly all Fe_3O_4 . A total of 7 areas on different

wires were analyzed. All spectra show the most common species observed were Fe_2O_3 and Fe_3O_4 . Three areas analyzed showed amorphous carbon.

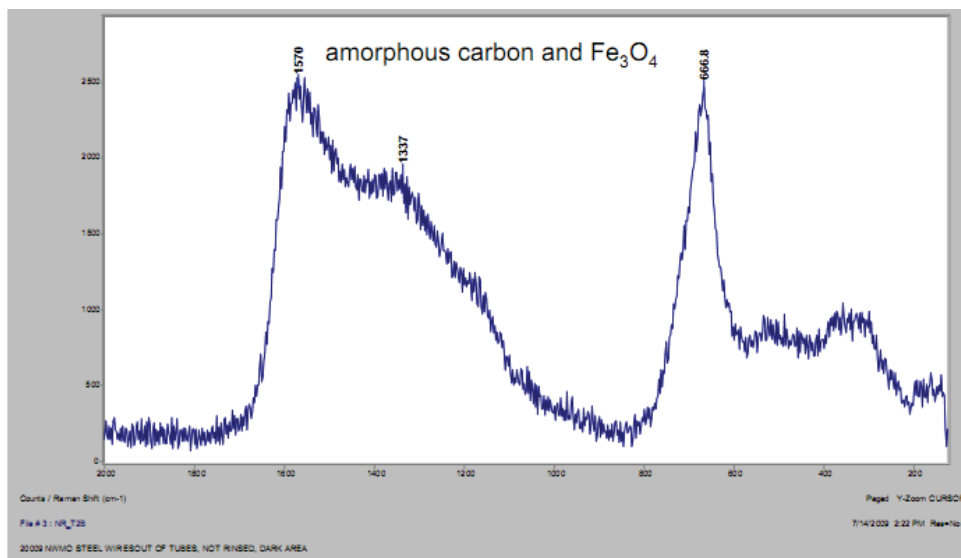


Figure 40 a: Raman spectrum of Sample 6 - 0.5M NaCl coated wires, 50°C, 75% RH (no rinse)

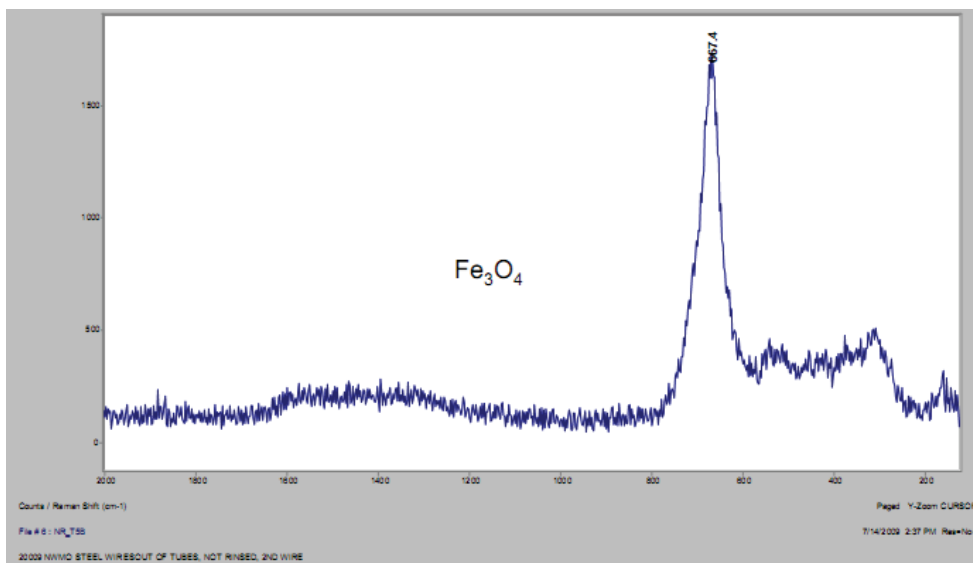


Figure 40 b: Raman spectrum of Sample 6 - 0.5M NaCl coated wires, 50°C, 75%RH

FTIR gave useful information on the thicker films formed on salt-coated samples. As shown in Figure 41, FTIR indicated the likely presence of a mixed carbonate / hydroxide species on the surface.

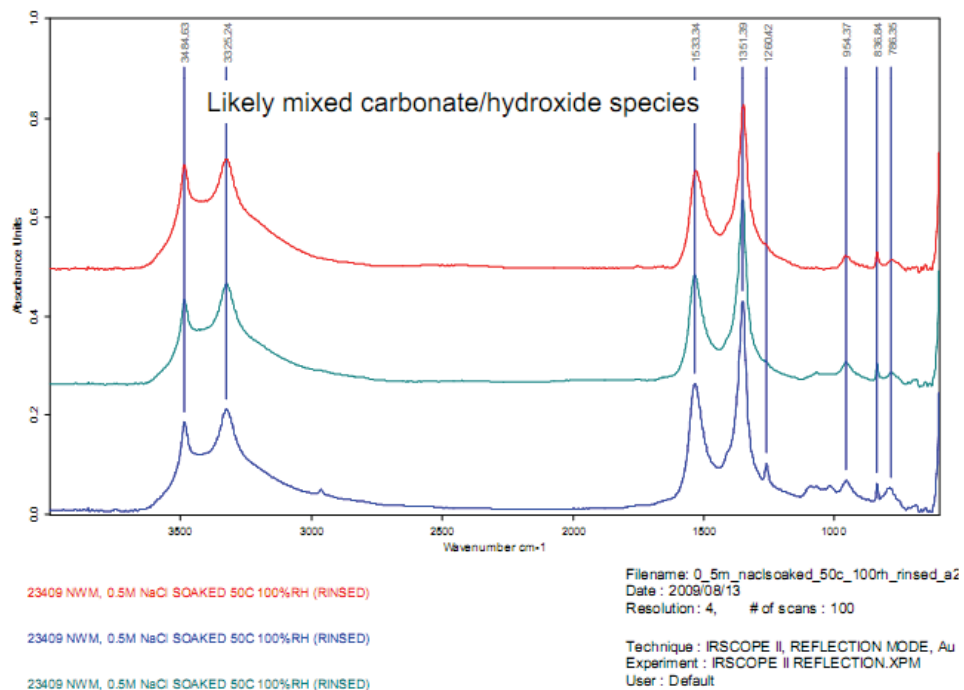


Figure 41: FTIR spectrum of Sample 10 – 0.5M NaCl coated wires, 100% RH, 50°C (rinsed)

Films formed at higher temperatures in anoxic conditions without a salt coating showed very well-resolved magnetite Raman spectrum – Figure 42a. A total of six (6) areas were analysed and all analyzed areas overlay nicely which showed significant consistency between the spectra. All spectra indicate the presence of Fe_3O_4 with some contribution from amorphous carbon. The six (6) spectra were averaged and the averaged spectrum is shown in Figure 42b, which clearly shows the dominance of magnetite.

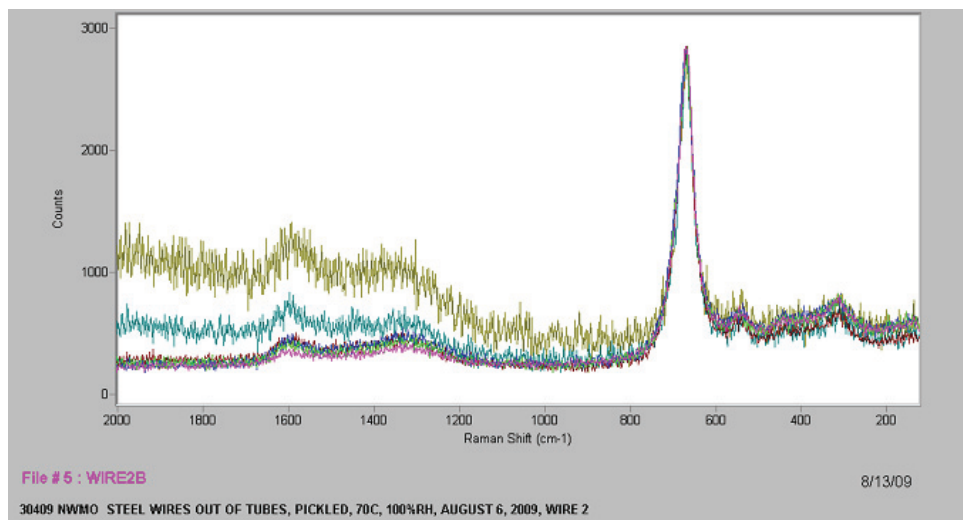


Figure 42 a: Raman spectrum of Sample 11 - pickled wires, 70°C, 100% RH

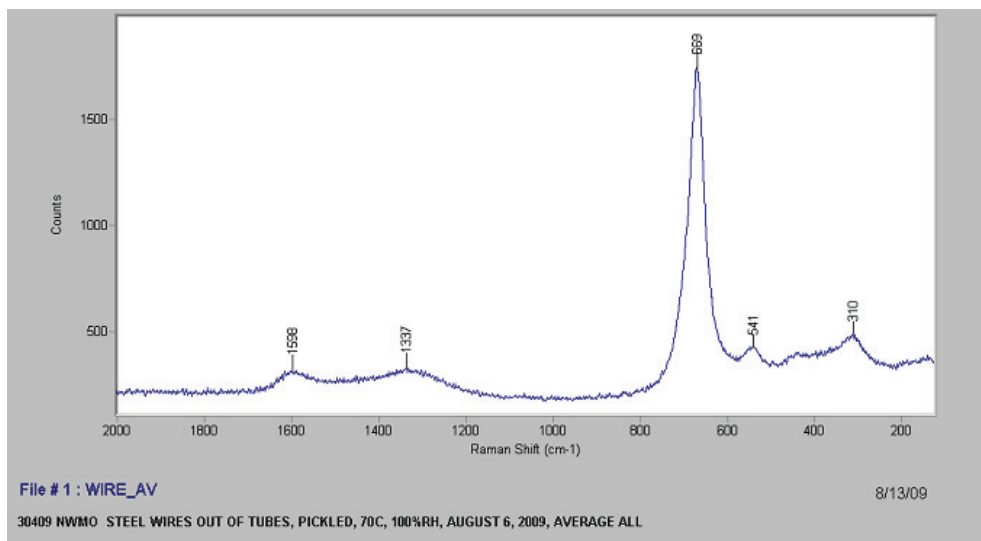


Figure 42 b: Raman spectrum (average) of Sample 11 - pickled wires, 70°C, 100% RH

5. FURTHER DISCUSSION AND CONCLUSIONS

The corrosion tests show that corrosion is persistent with massive salt deposition, likely to stabilize in the range $0.01\text{-}0.1\ \mu\text{m}\cdot\text{y}^{-1}$, but becomes extremely slow without salt deposition, even at 75-100% RH and 50-70°C. Future research using longer-term testing should be able to establish very favourable outcomes for certain parameter ranges. If we take the final corrosion rates in our tests as our benchmark for thinking about the repository, and speculate on informal extrapolations (recognizing the possibility of a change in corrosion mechanism with time), then at 50°C, and 100% or 75% RH, there is a very good chance that the corrosion rate will fall below $1\ \text{nm}\cdot\text{y}^{-1}$ within a year or so.

We understand, though, that newer concepts for the repository design may entail temperatures of up to 120°C. Further research will be required to determine whether or not the stifling of corrosion by the corrosion product persists at such temperatures, but the results already obtained at 70°C are promising in that respect.

Further work would be required to study the effect of the amount of salt deposit on the long-term corrosion rate. We obtained the surprising result that chloride was not purely catalytic, as it is in phenomena such as filiform corrosion of coated steel (Williams and McMurray, 2003) but became much less influential for only an order of magnitude reduction in the surface loading of chloride. The mechanism of this effect needs further research.

The Raman spectroscopy results have shown that magnetite is a predominant low-temperature product, contrary to what one might conclude from the literature. The sensitivity of the Raman method was very satisfactory. This crystallization of magnetite on the surface, analogous to protective films formed in hot water environments, is a favourable outcome for the protection of the metal, compared with the looser $\text{Fe}(\text{OH})_2$ type of film, although the Raman inactivity of the latter, together with imperfect air exclusion during sample transfers, makes the interpretation somewhat complex. X-ray photoelectron spectroscopy (XPS) analysis supports the presence of significant hydroxide in the products, although this can be ambiguous as the outer surface is always hydroxylated and contaminated with carbon; generally XPS is more useful for thin, invisible films as formed in some of the milder environments. In future, better sample transfer protocols can be developed in collaboration with surface science experts. Further combined use of Raman and XPS (with sputter etch profiling) is recommended, including spatially resolved studies such as examination of corrosion at sulfide inclusions.

Significant technical advances have been made. Before this work, it was not recognized that a simple pressure gauge could be used to measure corrosion rates down to $0.01\ \mu\text{m}\ \text{y}^{-1}$. Then, the introduction of the electrochemical hydrogen sensor has enormous promise, should even lower corrosion rates be of interest in future studies. It is already being used in research for the Swiss nuclear waste co-operative.

6. THE WAY FORWARD

This research points towards the following priorities for the further elucidation of the anoxic, atmospheric corrosion of carbon steel:

Longer-term testing under specific conditions of particular interest, expecting useful rate laws to emerge, supported by results of surface analysis and appropriate modelling.

Investigation of the effect of the amount (areal loading) of various salts on anoxic corrosion, and its explanation in terms of sequestration of anions by corrosion products, or other processes.

Further development of the electrochemical hydrogen sensor for estimation of very low corrosion rates, including the circumvention of the Pd membrane problem.

Exploitation of the very promising and surprisingly sensitive performance of the Raman microscope for further studies of film development, including improvement of transfer procedures for the avoidance of oxidation and drying of delicate corrosion products.

Similar improvements with respect to XPS, using 'vacuum suitcase' technology.

REFERENCES

- Henry, C. 1996. Measuring the Masses: Quartz Crystal Microbalances. *Anal. Chem. News and Features*, October 1996, pg. 626A.
- King, F. 2007. Overview of a Carbon Steel Container Corrosion Model for a Deep Geological Repository in Sedimentary Rock, NWMO TR-2007-01.
- Lewis, F.A. 1967. *The Palladium Hydrogen System*. London Academic Press.
- Lide, D.R. 2007-2008. *Handbook of Chemistry and Physics*, 88th Ed, CRC Press.
- Lyon, S.B. and D.J. Fray, 1983. Hydrogen Measurements using Hydrogen Uranyl Phosphate Tetrahydrate, *Solid State Ionics*, 9 and 10, pg. 1295.
- Mazurek, M. 2004. Long-Term Used Nuclear Fuel Waste Management – Geoscientific Review of the Sedimentary Sequence in Southern Ontario. Background Paper 6-12 prepared by Rock-Water Interactions, Institute of Geological Sciences, University of Bern for the Nuclear Waste Management Organisation. (Available at www.nwmo.ca)
- McMurry, J., D.A. Dixon, J.D. Garroni, B.M. Ikeda, S. Stroes-Gascoyne, P. Baumgartner, and T.W. Melnyk. 2003. Evolution of a Canadian deep geological repository: Base Scenario. Ontario Power Generation Report, 06819-REP-01200-10092-R00.
- Odziemkowski, M.S., T.T. Schuhmacher, R.W. Gillham, and E.J. Reardon. 1998. Mechanism of Oxide Film Formation on Iron in Simulating Groundwater Solutions: Raman spectroscopic studies. *Corrosion Science*, Vol. 40, No. 2/3, pg. 371-389.
- Peat, R., S. Brabon, P.A.H. Fennell, A.P. Rance, and N.R. Smart. 2001. Investigation of Eh, pH and Corrosion Potential of Steel in Anoxic Groundwater. SKB Technical Report TR-01-01.
- Smart, N.R., A.P. Rance and P.A.H. Fennell. 2006. Expansion due to the Anaerobic Corrosion of Iron. SKB Technical Report TR-06-41.
- SSW, University of Western Ontario. 2010. Surface Analysis of Carbon Steel Wire Specimens (not issued)
- Sullivan, C.K. and G.G. Guilbault. 1999. Commercial Quartz Crystal Microbalances – Theory and Applications. *Biosensors and Bioelectronics* Vol. 14, pg. 663-670.
- Williams, G. and H. N. McMurray. 2003. The Mechanism of Group (I) Chloride Initiated Filiform Corrosion on Iron. *Electrochemistry Communications*. Vol. 5, Issue 10, pg. 871-877.
- Winston, P.W. and D. H. Bates. Saturated Solutions for the Control of Humidity in Biological Research. *Ecology* Vol. 41, No. 1, pg. 232-237.

APPENDIX A: Leak test results

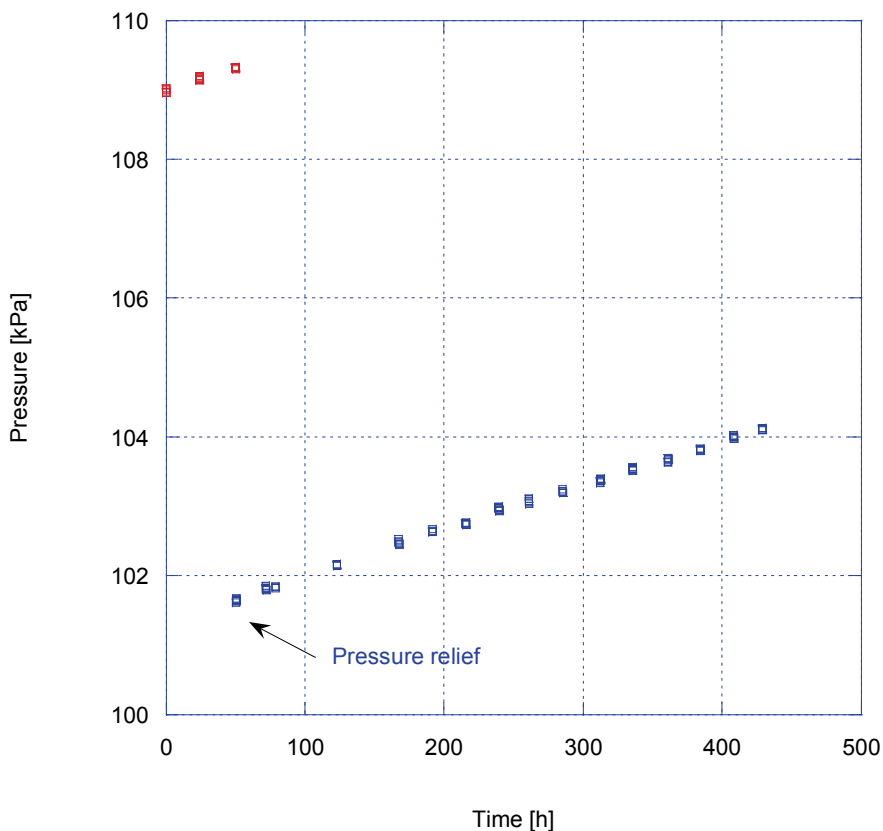
Leak Test (I)

Procedure

1. Place ~ 25 mL of deionized water into the lower compartment of an assembled test cell.
2. Deaerate the deionized water by purging with high purity nitrogen (99.999%) for 2 hours.
3. Continue deoxygenation of the vapour space of the glass cell using $N_2-5\%H_2$ for another 30 minutes.
4. Seal all openings with vacuum grease.
5. Place the assembled cell in the water bath set at $32^\circ C$.
6. Monitor pressure and temperature of the glass cell.

Volume of test cell: 168 mL
Volume of deionized water 23 mL
Test temperature $32^\circ C$

Figure A1 Leak Test (I)

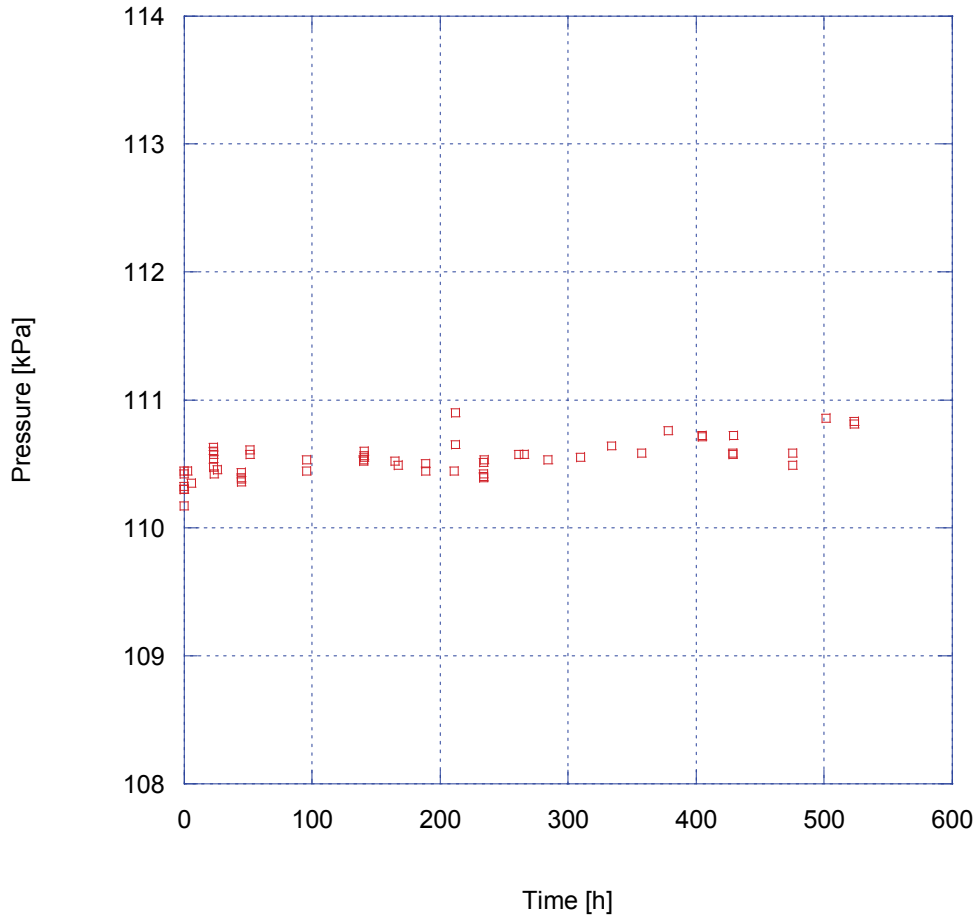


Note: steady pressure increase observed in the first leak test which was likely caused by unsteady temperature control. To improve temperature control, the water bath was covered with foam board to reduce evaporation and additional leak tests were performed to verify the suspected error.

Leak Test (II)

Volume of test cell: 166 mL
Volume of deionized water 26 mL
Test temperature 37°C

Figure A2 Leak Test (II)

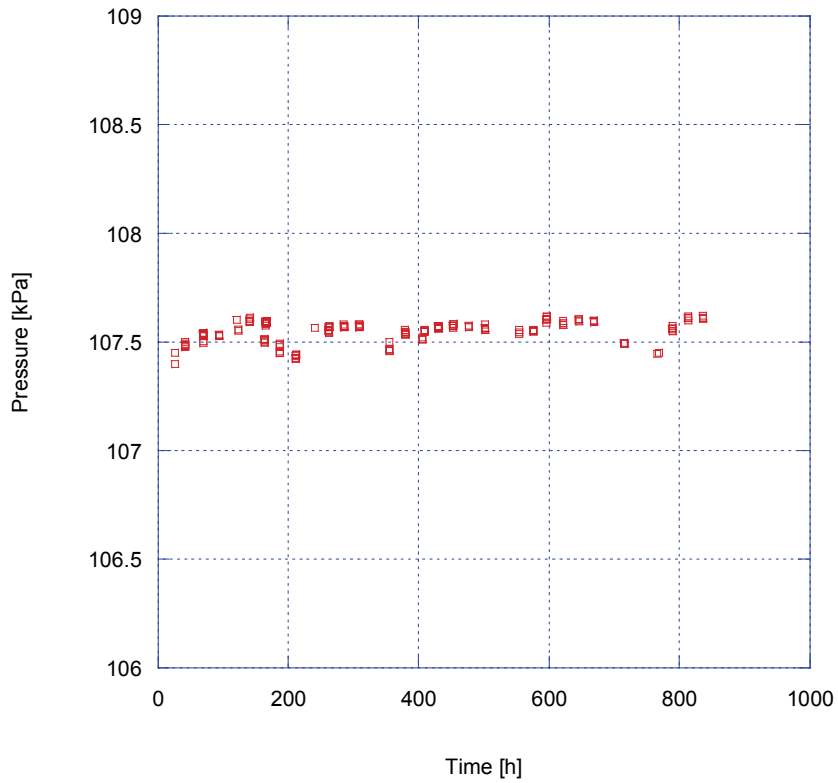


Note: Relatively stable pressure indications were obtained in the second leak test, suggesting proper sealing and air tightness of the glass cell.

Leak Test (III)

Volume of test cell: 167 mL
Volume of deionized water: 27 mL
Test temperature: 32°C

Figure A3 Leak Test (III)



Note: Similar to leak test (II), pressure was stable for over 800 hours, confirming the glass cell was sealed and gas leak tight.

APPENDIX B: Estimate of corrosion depth corresponding to a pressure change of 0.1 kPa

$$\text{Moles of hydrogen produced} = \frac{0.1\text{kPa} * 0.17\text{L}}{101.3\text{kPa} * 22.4\text{L}} = 7.5 \times 10^{-6} \text{ moles}$$

Moles of iron corroded per mole of hydrogen produced: 7.5×10^{-6} moles
(assuming corrosion product is $\text{Fe}(\text{OH})_2$)

$$\text{Moles of iron corroded per cm}^2 = 7.5 \times 10^{-9} \text{ moles}$$

Molecular weight of iron = 55.8 g/mol

$$\text{Grams of iron corroded per cm}^2 = 4.2 \times 10^{-7} \text{ g}\cdot\text{cm}^{-2}$$

$$\text{Density of iron} = 7.9 \text{ g}\cdot\text{cm}^{-3}$$

$$\text{Depth of iron corroded} = 4.2 \times 10^{-7} \text{ g}\cdot\text{cm}^{-2} / 7.9 \text{ g}\cdot\text{cm}^{-3} = 0.53 \text{ nm}$$

APPENDIX C: Quartz Crystal Microbalance (QCM) Testing

In an attempt to monitor changes of mass of the steel wires during the corrosion tests, a QCM200 Quartz Crystal Microbalance manufactured by Stanford Research Systems was used. The QCM200 measures mass and viscosity in processes occurring at or near surfaces, or within thin films. It is a stand-alone instrument with a built-in frequency counter and resistance meter. The instrument reads the resonant frequency and resistance of a 5 MHz, AT-cut quartz crystal.

The planned method for using the QCM200 was as follows:

1. Expose the crystal, coated with iron by vacuum deposition or electroplating, to a gaseous environment of particular relative humidity.
2. Measure the change of the crystal frequency with time, for which a meaningful duration would be 1-3 days. Superficial corrosion of the iron film will produce some corrosion product like $\text{Fe}(\text{OH})_2$, along with hydrogen, and cause mass change of the iron film.
3. QCM can measure the mass change on the crystal surface by the equation:

$$\Delta f = -C_f \Delta m \quad [1]$$

where Δf – the observed frequency change in Hz;
 Δm – the change in mass per unit area
 C_f – the sensitivity factor for the crystal

C_f is $56.6 \text{ Hz} \cdot \mu\text{g}^{-1} \cdot \text{cm}^2$ in a dry gas environment for the crystal we used at room temperature, but its value is affected by the environment and appropriate calibration is required. For our testing at 30°C , and relatively high humidity, C_f needs to be re-calibrated, using for example a silver or copper thin film.

It turns out that for a corrosion rate of ca. $0.01 \mu\text{m} \cdot \text{y}^{-1}$, the QCM is adequately sensitive if well calibrated, but (omitting the details of many tedious investigations) has a day-to-day drift, especially in humid conditions, that swamps the signal from the corrosion reaction, far beyond any possible effect (1 Hz or so) of temperature fluctuation – Figure C1.

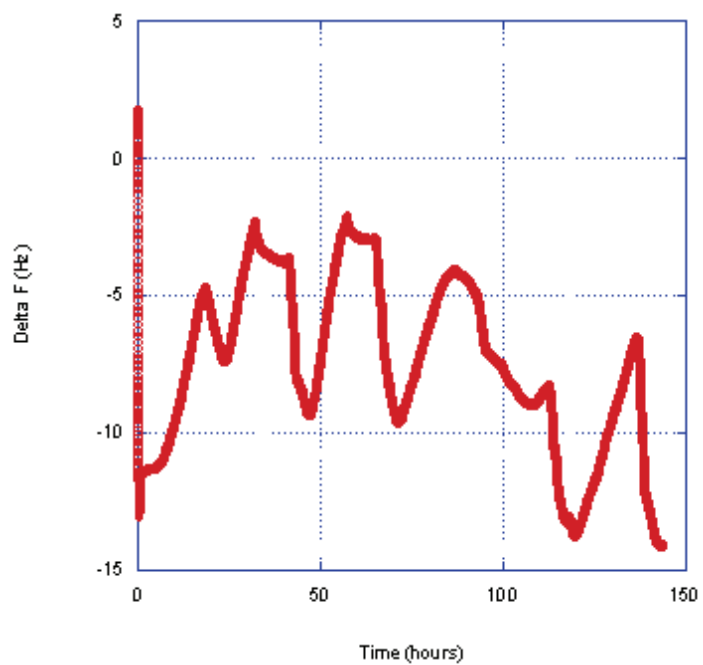


Figure C1: Change of the frequency of the crystal without any deposit in an environment of 100% RH at 30°C

APPENDIX D: Preparation of the palladium membrane

Date	Conditions Evaluated	Observations
Jun 04, 09	<ul style="list-style-type: none"> ▪ Mounted a 100 µm thick Pd foil between the upper and lower compartment. ▪ Filled the lower compartment with a H₂ / N₂ mixture for 20 minutes and measured H₂ via the outlet valve of the copper cell using the H₂ sensor at different time intervals. 	<ul style="list-style-type: none"> ▪ 2 hours after the injection, no H₂ was detected in the upper compartment of the Cu cell. ▪ 20 hours after the injection, no H₂ was detected.
Jun 05, 09	Repeated above test at 50°C	<ul style="list-style-type: none"> ▪ No H₂ was detected.
Jun 12, 09	<ul style="list-style-type: none"> ▪ Heat treated the Pd membrane (prior to mounting inside the copper cell) by baking the Pd membrane at 600°C for 1 hour and allowed to cool to room temperature ▪ The assembled copper cell was then placed in the water bath set at 50°C. 	<ul style="list-style-type: none"> ▪ H₂ was measured after 18 hours, no H₂ was detected in the upper compartment of the Cu cell.
Jun 21, 09	<ul style="list-style-type: none"> ▪ Heat treated the Pd membrane at 720°C for ½ hour and left in oven set at 500°C for several hours, and then allowed to cool to room temperature inside a crucible (the crucible was pre-filled with 100 ppm H₂ / N₂ mixture). ▪ The assembled copper cell was then placed in the water bath set at 50°C. 	<ul style="list-style-type: none"> ▪ H₂ was measured after 17 hours, no H₂ was detected in the upper compartment of the Cu cell.
Jun 24, 09	<ul style="list-style-type: none"> ▪ Heat treated the Pd membrane at 720°C for ½ hour and left in oven set at 500°C for several hours, and then allowed to cool to room temperature in air for another several hours. ▪ The foil was then placed in a tube furnace set at 200°C for 30 minutes. During this period, the tube furnace continued to be flushed with Ar + 2.5% H₂. ▪ The assembled copper cell was then placed in the water bath set at 50°C. 	<ul style="list-style-type: none"> ▪ The Pd foil showed a greenish dark colour during the cooling in air period. ▪ The membrane showed a silvery white colour after heated in the tube furnace at 200°C. ▪ H₂ was measured after 17 hours, no H₂ was detected in the upper compartment of the Cu cell.
Jul 24	<ul style="list-style-type: none"> ▪ Annealed the Pd membrane in a crucible at 900°C for 1 hour ▪ Cooled in an oven set at 500°C for several hours, and then further cooling to room temperature in air. ▪ Coated the exit side of the Pd foil with 0.1M NaOH. ▪ Mounted the Pd membrane between the 2 compartments of the copper cell. ▪ Flushed the lower compartment with 100 ppm H₂ (balance with N₂) mixture for 30 minutes. ▪ Placed the assembled copper cell into a 50°C water bath. 	<ul style="list-style-type: none"> ▪ H₂ was measured 70 hours later, no H₂ was detected in the upper compartment of the Cu cell.

APPENDIX E: Sample calculation of film thickness estimation of Fe₃O₄ based on pressure measurement

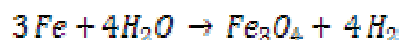
Pressure data for Sample 5 – Pickled wires exposed to 50°C, 100%RH is used to illustrate how the film thickness of Fe₃O₄ is estimated

Pressure detected: 4.8 kPa (from Figure 26)

Assume pressure measured = amount of hydrogen evolved, no. of moles of hydrogen is calculated using the ideal gas law.

No. of moles of H₂ in 0.14 L corrosion cell at 50°C = 2.45 x 10⁻⁴ moles

H₂ is generated in the following reaction:



No. of moles of Fe₃O₄ = 6.1 x 10⁻⁵ moles

Molecular weight of Fe₃O₄ = 231.4 g/mol

Mass of Fe₃O₄ = 0.014 g

Assume density of Fe₃O₄ = 5.1 $\frac{g}{cm^3}$

Volume of Fe₃O₄ = 0.0027 cm³

For surface area of 0.1 m², film thickness of Fe₃O₄ = $\frac{0.0027 \text{ cm}^3}{0.1 \text{ m}^2} = 27 \text{ nm}$